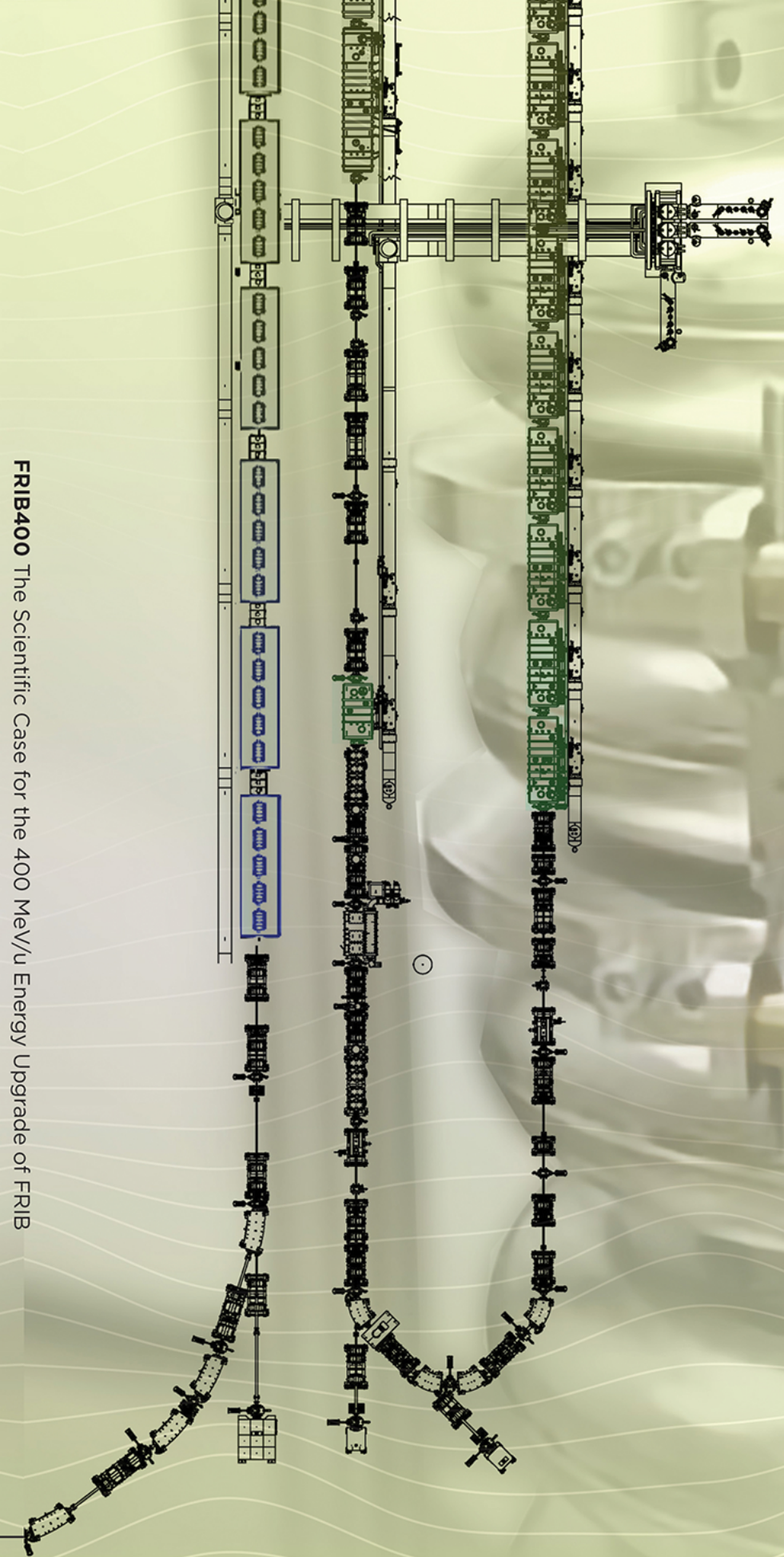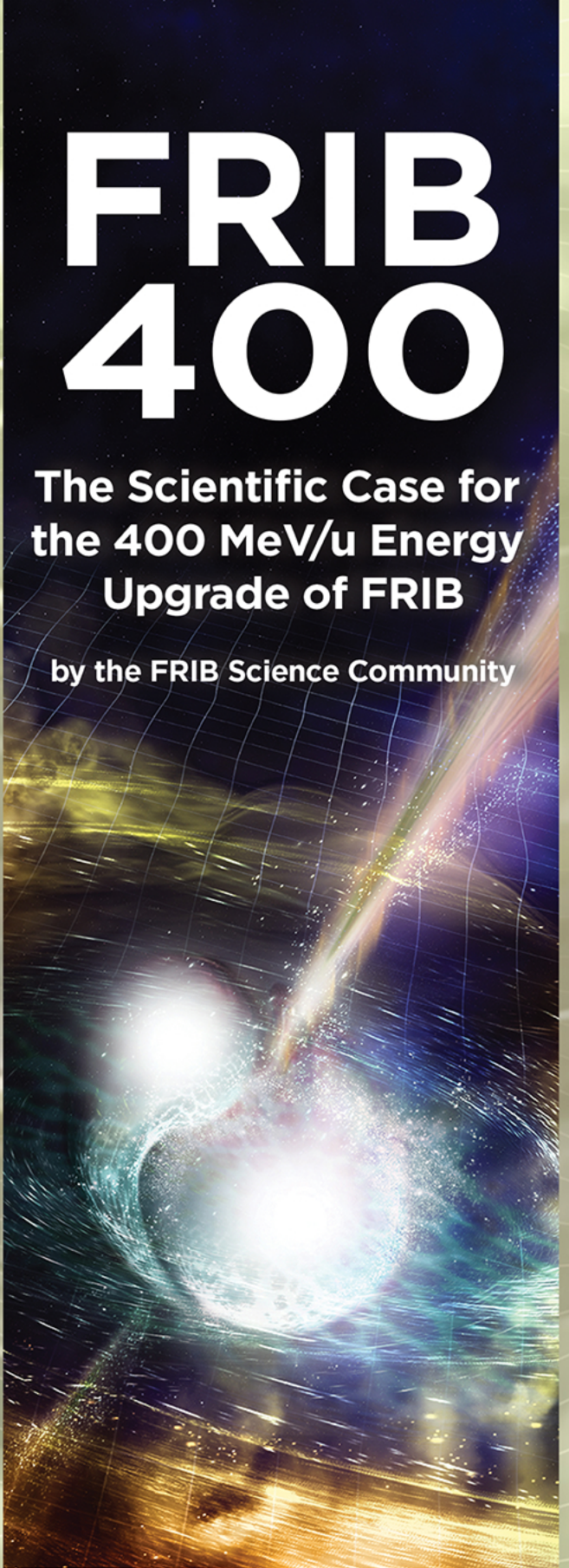# FRIB 400

The Scientific Case for the 400 MeV/u Energy Upgrade of FRIB

by the FRIB Science Community

FRIB400

The Scientific Case for the 400 MeV/u Energy Upgrade of FRIB

by the FRIB Science Community

Table of contents

Preface

A workshop *"Science with a 400 MeV/u upgrade of FRIB"* was held in August of 2018 in conjunction with the annual Low Energy Community Meeting (see the Appendix 1 to this document). The following resolution was adopted unanimously at the workshop and endorsed during the community meeting:

> *"We strongly support pursuit of the 400 MeV/u energy upgrade of FRIB. It will open new scientific opportunities and is timely given the recent neutron-star merger observation."*

Following the workshop, participants and others from the broader science community initiated preparation of this whitepaper (see Appendix 1 and 2 for contributors). The document presented here is the result of this community effort.

Executive summary

The energy upgrade of the FRIB linear accelerator to 400 MeV/u for uranium (FRIB400) will expand the already broad scientific reach of FRIB to encompass the full range of science envisioned by the scientific community and articulated in NSAC Long Range Plans and studies by the National Academies of Sciences. The scientific gains from FRIB400 above those to be realized initially at FRIB are significant and diverse: (i) Dense nuclear matter can be created and studied up to twice saturation density, critical for multi-messenger astrophysics; (ii) significant gains in isotope yields will be realized, nearly doubling the reach of FRIB along the neutron dripline and allowing study of extreme, neutron-rich nuclei; (iii) in experiments, thicker targets can be used, increasing the luminosity for measurements of nuclei in key regions of the nuclear chart; and (iv) nuclear reactions can be performed in an energy regime of optimum nuclear transparency, improving their interpretation by reaction theory.

The need for the FRIB400 upgrade has been made timely by the dawn of multi-messenger astronomy and the detection of gravitational waves and subsequent follow-up observations of electromagnetic radiation. The extremely neutron-rich environment of a neutron-star merger indicates that study of the most neutron-rich isotopes, many of which can only be made in sufficient quantities at 400 MeV/u, is necessary to understand *r*-process nucleosynthesis in a merger environment. Moreover, the gravitational-wave signature and amount of material ejected depend on the equation of state of very neutron-rich asymmetric nuclear matter at twice normal nuclear density, which can only be formed in the laboratory in nuclear collisions with rare isotopes at energies of 400 MeV/u or above.

An additional benefit of FRIB400 will be access to the neutron dripline over twice the range possible at FRIB. Insight into the nuclear many-body system and discovery of key physics have come from the study of the most exotic isotopes near the driplines or in regions of rapid structural changes. Regions that are now emerging as important, such as the heaviest calcium isotopes, will be opened for exploration at FRIB400. For all isotopes, higher-energy beams will enable the use of a broader range of nuclear reactions, reaching a region of maximum nuclear transparency with minimum distortions. The higher energy will allow for a more reliable study of weak-interaction processes in nuclei and allow for a more accurate determination of important nuclear properties such as neutron skins.

In anticipation of the science potential, as early as in the conceptual design stage of FRIB, space was provided in the FRIB tunnel for an energy upgrade of the accelerator to 400 MeV/u for uranium. The upgrade can be implemented with minimal or no interruption of the FRIB science program. A cavity and cryomodule design for FRIB400 was completed and prototyping is underway. The FRIB fragment separator and the beam distribution to key detector systems are well matched to the upgrade. Instruments, such as the High Rigidity Spectrometer, have been designed to be compatible with this upgrade.

Introduction

The Facility for Rare Isotope Beams (FRIB) will be the world's premier rare-isotope beam facility. It will make the majority (~80%) of the isotopes predicted to be bound available for experiments. These isotopes will allow researchers to understand atomic nuclei and their role in the Universe. The tremendous discovery potential of FRIB can be further extended with an energy upgrade of the FRIB linear accelerator to 400 MeV/u for uranium and to higher energies for lighter ions (FRIB400). This document outlines the outstanding and timely scientific opportunities made possible by FRIB400.

U.S. Department of Energy Office of Science Office of Nuclear Physics mission is accomplished by supporting scientists who answer overarching questions in major scientific thrusts of basic nuclear physics research			
Science Drivers from the National Research Council (NRC) Rare-Isotope Science Assessment Committee (RISAC)			
Nuclear Structure	**Nuclear Astrophysics**	**Tests of Fundamental Symmetries**	**Applications of Isotopes**
Intellectual challenges from 2013 NRC Decadal Study and the 2015 NSAC Long Range Plan			
How does subatomic matter organize itself and what phenomena emerge?	How did visible matter come into being and how does it evolve?	Are fundamental interactions that are basic to the structure of matter fully understood?	How can the knowledge and technological progress provided by nuclear physics best be used to benefit society?
Specific questions included in the challenges			
What is the nature of the nuclear force that binds protons and neutrons into stable nuclei and rare isotopes? What is the origin of simple patterns in complex nuclei?	What is the nature of neutron stars and dense nuclear matter? What is the origin of the elements in the Cosmos? What are the nuclear reactions that drive stars and stellar explosions?	Why is there now more matter than antimatter in the Universe?	What are new applications of isotopes to meet the needs of society?
FRIB400 will help to answer the challenges formulated for the field			
17 Benchmarks from NSAC RIB TF measure capability to perform rare-isotope research, 11 will benefit from FRIB400			
1. **Shell structure** 2. Superheavies 3. **Skins** 4. Pairing 5. Symmetries 13. **Limits of stability** 14. **Weakly-bound nuclei** 15. **Mass surface**	6. **Equation of state (EOS)** 7. ***r* process** 8. $^{15}O(\alpha,\gamma)$ 9. ^{59}Fe supernovae 15. **Mass surface** 16. *rp* process 17. **Weak interactions**	12. **Atomic electric dipole moment**	10. **Medical** 11. **Stewardship**
FRIB400 will open new opportunities across all fields of rare-isotope science			

Figure: Science Drivers of rare-isotope science. The 400 MeV/u energy upgrade, FRIB400, will transform the study of 11 of the 17 Benchmarks (marked in bold) put forth by the Nuclear Science Advisory Committee (NSAC) Rare-Isotope Beam (RIB) Task Force (TF) to characterize the scientific potential of a rare-isotope facility [NSAC07].

At the dawn of multi-messenger astronomy, prompted by the observation of the neutron-star merger event GW170817, nuclear physics has emerged as one of the fields providing key physics insights into the merger process and its aftermath. In view of the importance of properties of extremely neutron-rich nuclei and compressed nuclear matter to neutron-star merger events, it is indeed timely to extend FRIB's scientific reach with an energy upgrade.

The exciting opportunities laid out in the following science sections include creating a density regime in heavy-ion reactions that is critical for determining the equation of state of nuclear matter and neutron stars; reaching more neutron-rich isotopes that are important for understanding the nucleosynthesis of the elements in the r process and in processes that occur in neutron-star crusts; accessing nuclei with extreme skins; providing the first spectroscopy of key nuclei that will guide theory and perhaps reaching the neutron dripline for crucial isotopic chains such as calcium.

FRIB400 would more broadly address the overarching intellectual challenges from the 2015 Nuclear Science Advisory Committee (NSAC) Long Range Plan [LRP15] and the National Research Council (NRC) Decadal Study [NaD13]. The drivers for rare-isotope science were evaluated and endorsed by the National Research Council's Rare-Isotope Science Assessment Committee (RISAC) [NRC07]. The upgrade would enhance the study of 11 of the 17 NSAC Rare-Isotope Beam (RIB) Task Force (TF) benchmarks [NSAC07], which were introduced to characterize the scientific potential of a rare-isotope facility as outlined in the RISAC report.

As early as during the conceptual design of FRIB, the scientific potential of FRIB400 was recognized and space was provided in the tunnel for an energy upgrade of the FRIB linear accelerator to 400 MeV/u. The magnetic rigidity of the corresponding rare-isotope beams is matched to the FRIB fragment separator and the high-rigidity beamlines envisioned to lead to the High Rigidity Spectrometer (HRS) [HRS] and the FRIB Decay Station [FDS]. Other beamlines could be upgraded if desired and opportune. The path for the technical implementation of FRIB400 is straightforward and allows for staging of the project without interruption of the FRIB science program.

FRIB400 is aligned with the U.S. Department of Energy Office of Science (DOE-SC) mission and has endorsement from the NSAC long-range planning exercises and the NRC studies. The DOE-SC mission of the Nuclear Physics (NP) program is to discover, explore, and understand all forms of nuclear matter that can exist in the Universe, including those that are no longer found naturally. As part of its mission, NP supports experimental and theoretical research, plans, constructs, and operates major scientific user facilities, and fabricates experimental equipment to serve researchers at universities, national laboratories, and industrial laboratories. The program provides world-class, peer-reviewed research results in the scientific disciplines encompassed by the Nuclear Physics mission areas under the mandate provided in Public Law 95-91 that established DOE-SC.

NP supports the DOE Strategic Plan [SP14] general goal of providing the world-class scientific research capacity needed to ensure the success of DOE missions in national and

energy security; to advance the frontiers of knowledge in physical sciences and areas of biological, medical, environmental, and computational sciences; and to provide world-class research facilities for the nation's science enterprise.

Specifically, an energy upgrade of the FRIB linear accelerator to 400 MeV/u supports Strategic Objective 3 *"Deliver the scientific discoveries and major scientific tools that transform our understanding of nature and strengthen the connection between advances in fundamental science and technology innovation."* Within NP, FRIB400 supports the goals of the low-energy nuclear physics program to understand atomic nuclei and their role in the Cosmos.

The possibility and value of this upgrade was recognized in the 2015 NSAC Long Range Plan—*"Space has been left in the linac tunnel to accommodate additional cryomodules, which would raise the production energy from 200 MeV/nucleon to 400 MeV/nucleon. This critical upgrade would increase the secondary beam yields by an order of magnitude."* FRIB400 realizes the vision of the 2002 NSAC Long Range Plan where the top priority for new construction was a rare-isotope facility *"providing beams from protons to uranium at energies of at least 400 MeV per nucleon, with beam power in excess of 100 kW."* The 2007 NSAC RIB TF commented that a facility such as FRIB400 *"...would undoubtedly have met the expectations of RISAC in full."*

1. Multi-messenger astronomy calls for higher FRIB beam energy

Science has entered a new era following the recent discovery of gravitational waves and high-energy cosmic neutrinos [Bar17]. It is the beginning of an age of multi-messenger astronomy where widely different observational data are recorded from astrophysical events. Interpretation of these disparate messages makes new demands on the underlying nuclear and particle science. It argues strongly that an upgrade of FRIB to 400 MeV/u beam energy is timely and necessary to address fundamental questions raised by the new data. The key is to have better access to the relevant rare isotopes that play a role in these extreme environments and to study nuclear matter under extreme conditions in nuclear reactions with sufficient energy to compress and probe nuclear matter at about twice nuclear saturation density, $2\rho_0$ [Rad18, Tsa19a]. In particular, because gravitational waves generated from neutron-star mergers are directly related to the equation of state (EOS) of nuclear matter [Abb17a, Abb18], the LIGO-Virgo collaboration's ground-breaking detection of the binary neutron-star merger event GW170817 has intensified efforts towards a comprehensive understanding of nuclear matter.

Moreover, nucleosynthesis in the extremely neutron-rich environment of matter emitted from a neutron-star merger proceeds through very neutron-rich isotopes of elements from iron to uranium [Mum16, Thi17]. Elucidation of the nucleosynthesis pathway is necessary to understand the role of neutron-star mergers as the site of the production of the heaviest elements in the Universe [Hor19, Cow19]. In extremely neutron-rich environments, fission recycling becomes relevant and an understanding of fission processes of very neutron-rich heavy nuclei becomes critical [Cot18]. Likewise, the neutrino flux from supernova explosions is related to the bulk properties of neutron-rich matter [Lat04, Rob12, Oer17].

The first observed multi-messenger event

The first multi-messenger event observed was supernova 1987a, where neutrinos were detected in coincidence with the regular electromagnetic display of a supernova (see e.g. [Bio87, Hir87]). The twenty or so neutrinos detected from this event gave credence to the theoretical picture of core-collapse supernovae that had been built over the preceding five decades and verified that a compact, hot, and dense young neutron star was present for at least twenty seconds in the center of the collapsed star. Today, a galactic core-collapse supernova would result in thousands of neutrino detections in multiple flavors (see e.g. [Mir16]). These neutrinos are emitted from hot, dense matter at around a hundredth to a tenth of nuclear saturation density and the time dependence of the supernova neutrino signal depends on the diffusion of neutrinos from supra-saturation density regions [Rob12, Bol17]. Therefore, the core-collapse supernova neutrino signal is directly shaped by the properties of nuclear matter. To interpret the implications of the next observed supernova signal for nucleosynthesis, neutrino physics, and the core-collapse supernova explosion mechanism itself, the properties of nuclear matter and weak-interaction rates need to be better constrained. FRIB400 will provide the necessary beam energy and rare-isotope yields to enable this work.

More generally, the nature of neutron stars, their crust, and layers, involve nuclear matter significantly more neutron-rich than normal matter and its properties are relevant for interpreting a wealth of astronomical data [Sch13, Oer17]. All of these observations point to the importance of the most neutron-rich isotopes and the need for FRIB400.

The following sections show that with the extended reach of 400 MeV/u beam production, FRIB400 will be poised to answer many of the key questions, such as: What do gravitational waves tell us about the neutron-matter EOS? What do neutrino signals reveal about supernova evolution? What do neutron-star cooling rates and astronomical X-ray data tell us about the structure of neutron stars? What are the sites of the r process and how does it proceed to produce the heavy elements?

1.1 The nature of neutron stars and the nuclear equation of state

The EOS of nuclear matter relates temperature, pressure, and density of a nuclear system. It governs not only properties of nuclei and neutron stars but also the dynamics of nucleus-nucleus collisions and neutron-star mergers. The EOS also determines the amount of ejected matter from a neutron-star merger, which subsequently undergoes nucleosynthesis to form heavy elements up to uranium and beyond [Ros99, Bov17, Kas17, Fuj18, Hor19]. The ultimate fate of a neutron-star merger is also impacted by the EOS, determining whether the colliding neutron stars collapse promptly into a black hole, remain a single neutron star, or form a transient neutron star that collapses later into a black hole [Bau17]. The recent observation of GW170817 demonstrated that the gravitational-wave signal from neutron-star merger events encodes the properties of nuclear matter and its EOS through the tidal deformabilities of the neutron stars during in-spiral [Abb17a, Zha18, Pie19, Car19].

FRIB400 will allow laboratory study of asymmetric nuclear matter at twice normal nuclear density. Understanding dense, neutron-rich matter is important for interpretation of multi-messenger data from neutron-star mergers.

Given this sensitivity, the interpretation of multi-messenger observations from neutron-star mergers and their nucleosynthesis therefore requires a better understanding of the nuclear EOS. This makes experiments with FRIB400, which can probe the important higher density regime, particularly timely. In addition, given that gravitational-wave signals from neutron-star mergers offer unique new opportunities to directly constrain the nuclear EOS for very neutron-rich matter, laboratory constrains from measurements with neutron-rich nuclei at FRIB400 will provide additional constraints that will yield opportunities for significant new insight and discovery.

While the temperature dependence of the EOS is important for the description of mergers after the neutron stars make contact [Rad16, Han17], it builds on the understanding of cold nuclear matter. The EOS of homogeneous, cold nuclear matter can be expressed in terms of the density-dependent energy of the system. In leading order, the energy per nucleon

Neutron-star and heavy-ion collisions

The long journey: Once upon a time, in a far-away galaxy, inside the constellation Hydra, two orbiting neutron stars performed the ultimate death spiral and merged. It took 130 million years for the gravitational waves generated by the merger to traverse the vast Cosmos to reach Earth. The signal detected by the LIGO-Virgo collaboration [Abb17b] lasted a mere 100 seconds but, triggered by the event, some 70 ground- and space-based observatories swung into action and ushered in an era of sophisticated multi-messenger astronomy. At a time of 1.7 seconds after the neutron stars merged, a γ-ray burst with jets of high-energy particles was detected by the Fermi Gamma-ray Space Telescope and confirmed by the INTEGRAL satellite. Guided by the triangulation of the LIGO-Virgo observation, several telescope teams observed a transient star called a kilonova [Kas17, Sma17] in the dark sky of South America some 10 hours later. In the subsequent days and weeks, the optical spectra [Arc17] of the kilonova shifted from ultraviolet to red, suggesting the presence of lanthanide-like elements and confirming the neutron-star merger as a possible nucleosynthesis site for neutron-rich *r*-process elements [Pia17]. Delayed X-ray [Tro17] as well as radio signals [Hal17] from the afterglow were discovered weeks later. Incidentally, neutrinos that were observed in the first multi-messenger astronomical event, supernova 1987A, were not detected for GW170817.

When two neutron stars are within a few hundred kilometers, they exert a significant tidal force onto each other. By measuring the
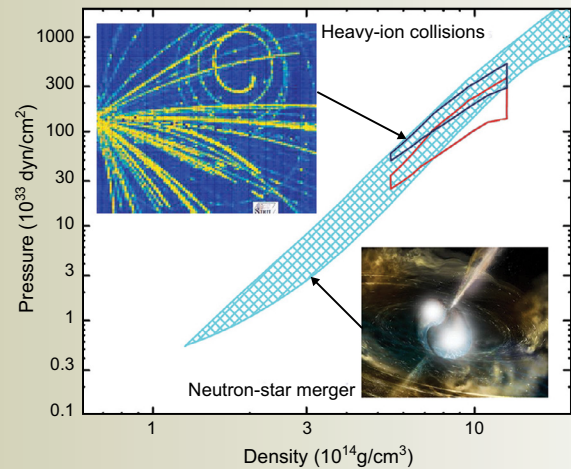
deformation of the neutron stars due to this tidal force, one can deduce how neutron-star matter reacts to pressure and density. The hatched blue region in the picture shows the pressure-density relationship, also known as equation of state (EOS), of nearly pure neutron matter deduced from the GW170817 observation [Abb18]. Sixteen years earlier, Danielewicz, Lacey, and Lynch deduced the pressure-density relationship from heavy-ion collision data for symmetric nuclear matter that has the same number of neutrons and protons [Dan02]. By assuming two "extreme" formulations of symmetry pressure, which contributes significantly to the core of a neutron star, they predicted the EOS of pure neutron matter, shown as two contours in the figure. Experiments at FRIB400 will be able to distinguish the two assumptions used in the formulations of the symmetry pressure which is critical to our understanding of the properties of neutron stars.

consists of two terms, one for symmetric nuclear matter ($E(\rho,\delta = 0)$, which is independent of the neutron-proton asymmetry) and a second one that is proportional to the square of the neutron-proton asymmetry:

$$E(\rho,\delta) = E(\rho,\delta = 0) + S(\rho)\delta^2$$

The asymmetry parameter $\delta = (\rho_n - \rho_p)/(\rho_n + \rho_p)$ specifies how proton- or neutron-rich the system is. Here, the densities ρ_n and ρ_p are the neutron and proton densities, respectively,

and $S(\rho)$ is the density-dependent symmetry energy (in the following, we will use $E_{sym}(\rho) = E(\rho,\delta) - E(\rho,\delta = 0) = S(\rho)\delta^2$ in leading order). The pressure resulting from the nuclear EOS is given by $\rho^2 \partial E(\rho,\delta)/\partial\rho$, which contains a contribution from symmetric nuclear matter, P_{SNM}, and a contribution from asymmetric matter, P_{sym}.

The term $E(\rho,\delta = 0)$ is constrained by data from heavy-ion collisions and bulk nuclear properties [Dan02, Lyn09, Rus16, Coz18]. The symmetry energy is less well constrained at supra-saturation densities, i.e., above nuclear saturation density. This is a reflection of uncertainties in nuclear interactions that are not adequately probed through study of the properties of nuclei at saturation density. Hence, in order to understand gravitational-wave signals, neutrino fluxes, and other astrophysical data, it is critical to probe the EOS at high densities and over a wide range of neutron-proton asymmetry.

During the in-spiral phase of a binary neutron-star merger, the gravitational field of each neutron star induces a tidal deformation in the other [Abb17a]. The influence of the EOS of neutron stars on the gravitational-wave signal during the in-spiral phase is encoded in the dimensionless, neutron-star tidal deformability, Λ [Abb17a]. A measurement of Λ can set constraints on the nuclear EOS. The EOS constraints obtained from GW170817 and those from laboratory experiments for symmetric matter are shown in Figure 1.1 [Tsa19b]. The blue-shaded area in the left panel shows the pressure of nearly pure neutron matter $P_{PNM} = \rho^2 \partial E(\rho,\delta \approx 1)/\partial\rho$ for the neutron-star environment versus density for $1 \leq \rho/\rho_0 \leq 6$ that is consistent with the GW170817 gravitational-wave observation [Abb18]. The pressure for symmetric nuclear matter $P_{SNM} = \rho^2 \partial E(\rho,\delta = 0)/\partial\rho$ has been constrained at $2 \leq \rho/\rho_0 \leq 4.5$ from collective-flow measurements in Au + Au collisions [Dan02, Lef16]
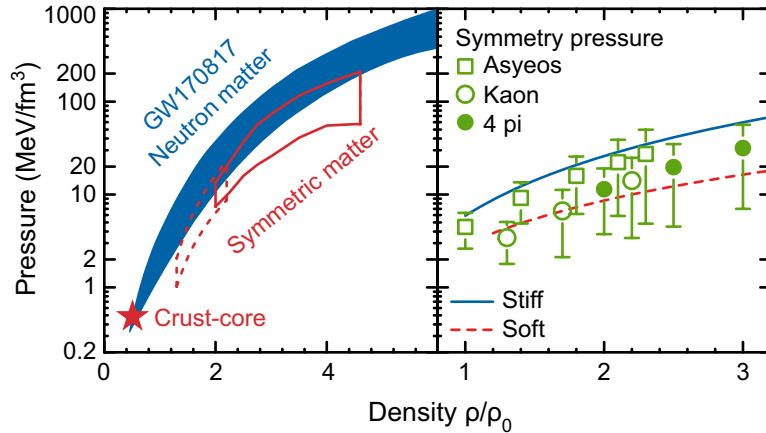
Figure 1.1: (Left) Experimental and astrophysical constraints on the EOS in pressure vs. density. The blue shaded region represents the gravitational-wave constraint on the pressure of pure neutron matter, P_{PNM}, at the 90% confidence level [Abb18]. The solid and dashed contours correspond to the pressure, P_{SNM}, at the 68% confidence level, of symmetric matter constraints extracted from flow [Dan02] and kaon measurements [Fuc06, Lyn09], respectively. The star marks the crust-core transition pressure extracted from symmetry-energy data below ρ_0 [Lyn18]. (Right) Density dependence of the symmetry pressure P_{sym} at supra-saturation density. Circles represent 50% confidence-level values for P_{sym} obtained from the difference of P_{PNM} and P_{SNM} shown in the left panel. Open squares are 68%-confidence-level values of P_{sym} obtained from neutron and proton elliptical flow data and analyses presented in references [Rus16, Coz18]. Figure adapted from [Tsa19a].

and at $1.2 \leq \rho/\rho_0 \leq 2.2$ from kaon-production measurements [Fuc06, Lyn09]. The contours marked by the red solid and dotted lines in Figure 1.1 (left) represent these constraints on the symmetric matter EOS. Assuming the most probable values lie at the centers of these contours, one can deduce the dependence of the symmetry pressure (resulting from a proton-neutron asymmetry), $P_{sym} = P_{PNM} - P_{SNM} = \rho^2 \partial E_{sym}(\rho)/\partial\rho$, and how it increases with density; this is shown by the open and filled circles (at the 50% confidence level) in Figure 1.1 (right) [Tsa19b]. Due to the large uncertainties in P, however, $P_{PNM} - P_{SNM}$ does not preclude negative P_{sym} at the 90% confidence level. Hence, the current results from GW170817 do not yet provide firm constraints on P_{sym}. Additional observations and improved information from nuclear collisions will better constrain P_{sym}. To provide a reference for the symmetry pressure, the red dashed line shows the symmetry pressure for a weakly density-dependent "soft" symmetry energy, and the blue line indicates strongly density-dependent "stiff" parameterizations for symmetry pressure within neutron stars from [Pra88].

Direct constraints on P_{sym} have been obtained from the differences between the elliptical flow of neutrons and protons emitted in Au + Au collisions at 400 MeV/u. These flow measurements provide constraints on the first and second derivatives of $S(\rho)$ [Coz18], providing the P_{sym} values indicated by the open squares in Figure 1.1. While more precise than the constraints obtained from P_{sym} with GW170817, the elliptical-flow constraints of [Coz18] nevertheless carry large uncertainties. With the availability of beams covering a wider range of the proton-neutron asymmetry δ and increased intensities at FRIB400, these uncertainties can be reduced by factors of 2 to 3 with heavy-ion reaction measurements.

To take advantage of the new data from gravitational-wave observations, and to inform multi-messenger observations, measurements at FRIB must probe the EOS under the appropriate conditions. Connections between the nuclear EOS and neutron-star properties are illustrated in Figure 1.2, which shows the relationship between the symmetry energy, pressure, and the neutron-star tidal deformability (which is also related to the neutron-star radius R). The open circles are calculations using various Skyrme energy density functionals [Tsa19a]. Figure 1.2 (left) shows that at sub-saturation densities, the correlation between symmetry energy and Λ (or R) is non-existent and there is no sensitivity to these neutron-star observables. This is consistent with findings of [Pie19, Car19] who concluded that tidal deformability only weakly depends on the EOS at $\rho \leq \rho_0$.

On the other hand, the trend exhibited in Figure 1.2 (right) reflects the fact that Λ and P are correlated and both are largely determined by the pressure near $2\rho_0$ [Abb18, Fat18, Zha18, De18]. The soft and stiff limits for $S(\rho)$, corresponding to the curves in Figure 1.1 (right), are shown as red and blue rectangles in Figure 1.2 (right). For example, tidal-deformability values in the range of 170 to 450 would be consistent with a soft symmetry energy (red), but not a stiff one (dark blue). An experimental determination of the symmetry pressure (such as stiff or soft) would, in turn, set stringent constraints on Λ and P and on the difference between neutron and proton chemical potentials within the star that are important for understanding its internal structure [Pet95, Bla05]. Moreover, the expected improvement in heavy-ion and in the gravitational-wave constraints will allow us to understand what

these combined constraints imply for the microscopic nature of strongly interacting matter within the neutron-star environment.

From Figure 1.2 it is clear that studies of nuclear matter at supra-saturation densities are critical. This is the density regime that is important to be probed at FRIB. As shown in Figure 1.3, such densities can be created in heavy-ion collisions provided that sufficient energy is available to compress the nuclear matter. The range between the green and the blue curves approximately corresponds to what will be possible at FRIB prior to the upgrade: the critical region of twice saturation density is not reached. The red curve shows the density and the time duration that could be probed with FRIB400: the critical range of densities is reached. Even higher densities will be achieved in complementary experiments at facilities such as the Facility for Antiproton and Ion Research (FAIR).
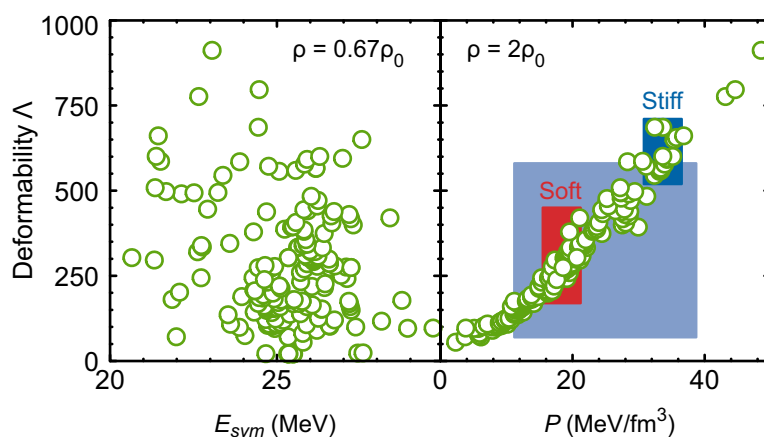

Figure 1.2: Neutron-star tidal deformability vs. symmetry energy at $0.67\rho_0$ (left) and vs. total pressure in neutron matter at a density of $2\rho_0$ (right). The light blue shaded region marks the constraint from GW170817. The extracted limiting stiff and soft constraints are represented by the dark blue and red shaded regions, respectively. The circles correspond to the respective correlation predicted by a number of Skyrme functionals [Tsa19a]. At low density, the tidal deformability only depends weakly on the EOS, while the correlation is strong at $2\rho_0$.

Experimentally, there are a number of observables from heavy-ion collisions that can probe the symmetry energy. These include the π^-/π^+ and n/p spectral ratios [Tsa17, Rei07] and differences between the transverse [Li00] and elliptical [Rus16, Coz18] flows of neutrons and protons in heavy-ion collisions at intermediate energies. The ratio of π^- to π^+ production is predicted to be a sensitive probe of the symmetry energy at high density [Tsa17]. Figure 1.4 shows transport-model predictions [Hon14] for π^- and π^+ production as a function of time in $^{132}Sn + ^{124}Sn$ collisions. As both Figures 1.3 and 1.4 correspond to the same calculation, it is evident that the pions are produced approximately when the peak densities are achieved. Very low sub-threshold pion yields are produced at the nominal FRIB beam energy of ~200 MeV/u. The increase in pion yield by more than a factor of 100 at ~450 MeV/u at FRIB400 as compared to FRIB will permit detailed explorations of pion production at densities in the vicinity of $2\rho_0$.

Constraints on both momentum-dependent and momentum-independent isovector mean-field potentials are also needed as they largely define the symmetry energy. The elliptical

flow results in Figure 1.1 illustrate the capability of elliptical flow to constrain the symmetry pressure. Impact-parameter dependencies of elliptical flow [Dan00] and of single and double n/p spectral ratios [Zha14] also provide means to constrain the momentum dependence of the isovector mean-field potential. Not only is FRIB400 necessary to reach densities up to $2\rho_0$, with FRIB400, the effect of the elliptical flow is larger and the model uncertainties decrease [Xu16].
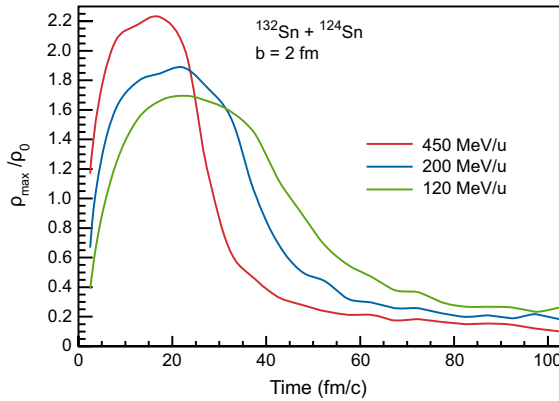

Figure 1.3: Maximum density reached in the collision of ^{132}Sn + ^{124}Sn for three different beam energies as a function of time predicted with the Boltzmann-Uehling-Uhlenbeck (BUU) model of [Hon14]. Early in the collision, the highest densities are reached. With FRIB400, the density range between the blue and red curves can be accessed.
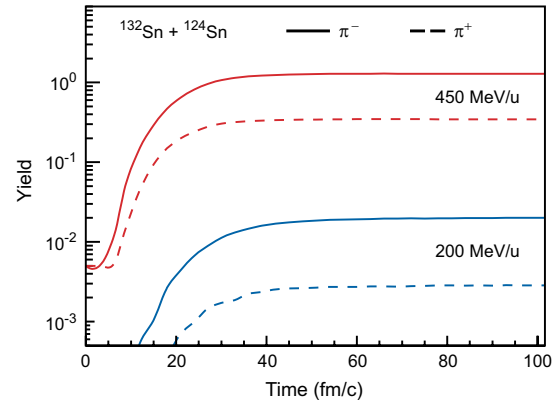
Figure 1.4: Integrated yield of charged pions as a function of time in heavy-ion collisions of ^{132}Sn + ^{124}Sn assuming a soft symmetry energy. The energy dependence of the charged pion production near threshold demonstrates that higher beam energy has a significant advantage for these experiments.

FRIB will have the highest intensity of neutron- and proton-rich beams in the world, enabling experiments with the widest range of δ to be explored. Studies of combined beam-plus-target systems over a wide range of δ are important to extract the symmetry-energy contribution with precision. For example, FRIB400 would have sufficient intensity for experiments with tin isotopes ranging from ^{104}Sn to ^{134}Sn on targets of ^{112}Sn to ^{124}Sn with δ ranging from approximately 0.05 to 0.25. In the case of the calcium isotopes, which can be accelerated to even higher energy, δ ranges from approximately -0.10 to 0.20 for experiments with ^{36}Ca to ^{52}Ca on targets of ^{40}Ca to ^{48}Ca.

In summary, experiments with FRIB400 will study matter under extreme conditions and set constraints on the symmetry energy and symmetry pressure within neutron stars. It will provide key information to interpret multi-messenger observations. The combination of multi-messenger constraints on the neutron matter EOS (from the radii and tidal deformability of neutron stars), combined with constraints on the symmetry energy and on the symmetric matter EOS, will reveal a detailed picture of the EOS of neutron-rich matter. These constraints will be confronted with the results of theoretical efforts to calculate the nuclear matter EOS from heavy-ion collisions and will provide a deeper understanding of nuclear forces. In addition to the insights into the symmetry energy that FRIB400 will provide, the associated density and momentum dependence of the isovector fields and the neutron-proton effective mass splitting, essential to understand thermal properties of neutron stars and their cooling via neutrino emission, will also be explored.

1.2 The nuclear force and nuclear matter equation of state

The measurements discussed in the previous section will more broadly provide key insights into the modeling of the nuclear force as they will pose constraints at high nuclear density or equivalently small nucleon separation. Specifically, the density dependence of the symmetry energy is associated with the uncertainty in how to model the short-range part of the nuclear interaction [Gan12, Heb13, Hag14, Gan15]. Hence, this dependence, which is a fundamental problem in nuclear physics, poses a stringent benchmark for models of nuclear interactions and energy density functionals. Density functional theory, which is at the heart of modern approaches to accurately model nuclei across the entire nuclear chart, can be constrained by the measurements discussed above [Erl13, Gor13, Che14].

Observables from the supra-saturation region would complement constraints obtained from low-energy nuclear observables. Figure 1.5, which serves as an example of related work in this area, illustrates this point. The solid curves are calculated with the Skyrme functional SV-min constrained by ground-state nuclear data (red) and by an imminent measurement of the neutron skin thickness in ^{208}Pb (blue and green corresponding to different assumed errors). Also shown are results of a relativistic mean-field model (RMF) in order to illustrate systematic uncertainties associated with other model assumptions. As shown in the figure, low-energy data such as the neutron skin of ^{208}Pb provide tight constraints in the low-density region around nuclear saturation. Beyond the region of the constraints, the extrapolated error grows rapidly. Other approaches can constrain the slope of the curves by using nuclear properties at around saturation [Li14, Bro17, Tew17], but do not accurately constrain the symmetry energy at appreciably higher densities.
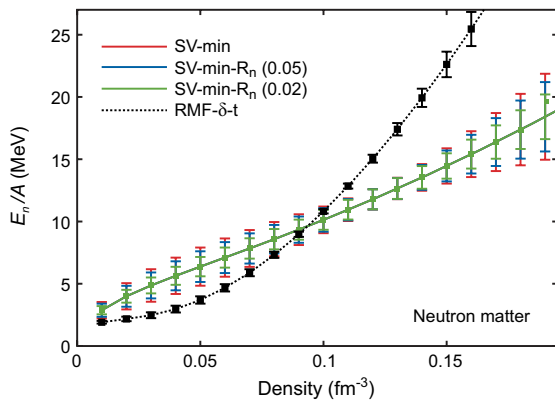
Figure 1.5: Extrapolation errors for the neutron matter EOS predicted by the energy density functional SV-min (obtained by a fit to the standard pool of low-energy nuclear data) and SV-min-R_n (obtained by adding to the data set the neutron radius, r_n^{rms} = 5.61 fm in ^{208}Pb with an adopted error of 0.02 fm and 0.05 fm, respectively, to show the impact of a precise neutron radius measurement of ^{208}Pb). The neutron EOS predicted by RMF-δ-t is also shown for comparison. Figure adapted with permission from [Rei10].
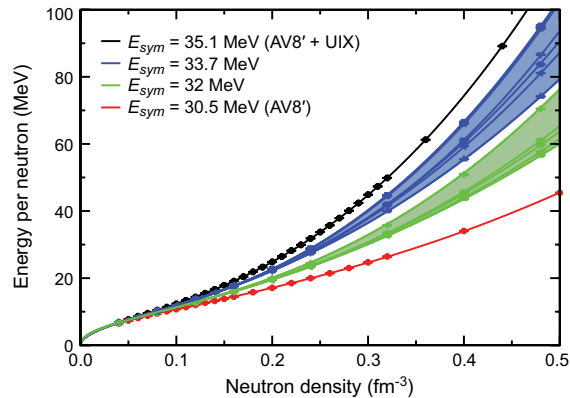
Figure 1.6: The EOS of neutron matter obtained by using various models of three-neutron forces in quantum Monte Carlo calculations [Gan15]. For each model, it is imposed that the energy at saturation is 17.7(1) MeV (blue band), or 16.0(1) MeV (green band). The results are compared with the EOS obtained with the AV8′ and AV8′ + UIX Hamiltonians. The legend indicates the corresponding symmetry energy at saturation. Figure adapted with permission from [Gan15].

Figure 1.6 shows quantum Monte Carlo calculation of the EOS with the AV8′ interaction and various models for the three-neutron interaction [Gan12, Gan15]. These calculations are adjusted to give the value for E_{sym} at saturation indicated in the figure and illustrate the difference between stiff and soft equations of state. The range of E_{sym} is compatible with the current experimental constraints. To obtain a lower symmetry energy with the AV8′ model of two-body interactions would require an attractive contribution of the three-body force. The three-body components give attraction in pure neutron matter, but they would require a strong short-range repulsion to make the EOS stiff enough to support astrophysical observations.

FRIB400 will allow the short-range part of the nuclear force to be studied.

Using the EOS obtained from different nuclear Hamiltonians as shown in Figure 1.6, a clear effect on neutron-star structure can be seen. The results are displayed in Figure 1.7, where neutron-star mass and radii corresponding to various EOSs are shown. Since the radii of neutron stars are mostly determined by the EOS around $2\rho_0$ [Lat01, Lat04, Rad18], future measurements are needed to provide strong constraints on the nuclear Hamiltonian and choose between the stiff (blue) or soft (green) parameterizations. In particular, as discussed in the previous section, the spectral ratio π^-/π^+ in charged-pion production during heavy-ion collisions is sensitive to this difference of soft and stiff. The red and black curves correspond to the EOS calculated with the AV8′ two-body interaction alone and to AV8′ with the UIX three-neutron potential, respectively. The relation between E_{sym} and the radius is evident, as an increase of E_{sym} predicts a neutron star with a larger radius. In the figure, the central density of the neutron matter inside the star is indicated with the yellow lines. For large masses, the radius of the neutron star is mainly governed by the EOS of neutron matter
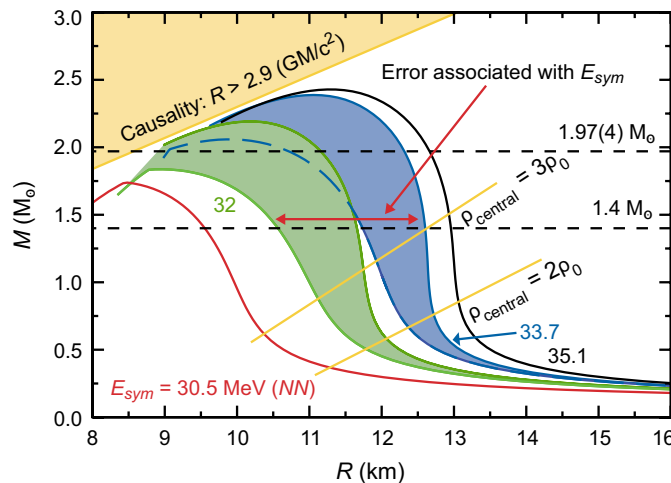
Figure 1.7: The mass-radius relation for neutron stars based on the quantum Monte Carlo neutron-matter results shown in Figure 1.6. Results are presented for the different EOSs as described in [Gan15] with observational constraints on the neutron-star mass from [Dem10]. The numbers indicate the value of E_{sym} of the various EOSs and reflect the uncertainty in the stiffness of the symmetry energy at higher density. Figure adapted with permission from [Gan15].

between ρ_0 and $2\rho_0$ [Lat01, Lat04, Rad18]. This illustrates the importance of understanding the origin and size of E_{sym} and its connection to the short-range behavior of the nuclear force.

1.3 Understanding the neutron-star crust

X-ray observations of the cooling of transiently accreting neutron stars (Figure 1.8) offer a unique window into the properties of dense matter for conditions not attainable in terrestrial laboratories [Mei18]. Using recent observations with space-based X-ray telescopes such as the Chandra X-ray Observatory or XMM Newton, comparisons of observations with models have revealed tantalizing hints of dense-matter physics. These include the identification of a mysterious, very strong source of heat (e.g. [Bro09, Tur15]), indications that nuclei at high density form an ordered, relatively pure, crystalline structure (e.g. [Rav83, Cac06, Cha08]), evidence for superfluid neutrons [Sht07, Bro09], and first constraints on the properties of nuclear pasta [Hor15, Dei17]—an exotic phase of dense matter predicted by nuclear theory but never observed. However, the models also reveal that the cooling behavior is inextricably linked to the properties of extremely neutron-rich nuclei present in the crust of the neutron star [Lau18]. FRIB will offer the first opportunity to determine these properties and identify which of these nuclei actually exist inside a neutron star. This will be essential to fully exploit observations and truly use accreting neutron stars as dense-matter laboratories for the multi-messenger era of astronomy. As shown below, FRIB400 is essential to achieve this goal.
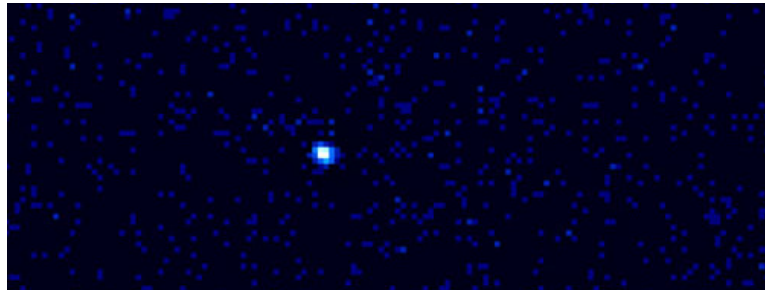
Figure 1.8: X-ray observations with the Chandra X-ray observatory of the transiently accreting neutron star KS1731-260. The neutron star was accreting matter from a companion star for about 12 years, making it a bright X-ray binary source. Accretion turned off in February 2001, resulting in a drop in luminosity by many orders of magnitude. The image shows the source within a month after accretion seized. The remaining dim glow is thought to be produced by the hot neutron-star crust, which was heated during the preceding 12 years of accretion. Surprisingly, the source then cooled significantly over the last 18 years. This, for a neutron star, very rapid cooling is explained by assuming that the crust is hotter than the bulk of the neutron star, and it is only the crust that is cooling. Credit: NASA/CXC/Wijnands *et al*. [Cha01].

The most striking feature of the observations of cooling neutron-star crusts after accretion has shut off is the rapid cooling with timescales of a few years. Such short timescales require a relatively pure crust with a relatively regular lattice structure that enables efficient heat transport. However, there is a problem with this scenario: the crust is formed from the ashes of X-ray bursts that occur frequently during the preceding accretion phase, and current theory predicts that the *rp* process [Wal81, Sch98] in X-ray bursts should produce a broad range of nuclei that would result in a very impure crust [Woo04, Jos10, Cyb16]. Recent model calculations have offered a possible explanation for this puzzle: during the

built-up of the crust from burst ashes, once nuclei have reached a depth where electron capture can transform them into extremely neutron-rich nuclei at the neutron dripline, electron-capture sequences with neutron emission, combined with neutron captures, rapidly drive the composition to lighter nuclei and concentrate the abundance in a few or a single species. In this picture, the outer crust is impure, but the inner crust—beyond the depth of where neutrons are released—is pure. The transition happens barely deep enough to be still consistent with observations.

FRIB400 will extend study of nuclei along the neutron dripline into a region important for modeling the crust of neutron stars.

However, irregularities in the pattern of nuclear masses along the reaction path that proceeds along the neutron dripline have been shown to stop the consolidation process; hence, a multi-component composition is retained to greater depth [Lau18]. For typical burst ashes, recent simulations have shown that this occurs at the traditional shell closures $N = 28$ and $N = 50$. Masses of $N = 50$ isotones around the neutron dripline play a critical role here. Current mass models predict a temporary strong concentration of abundance at $N = 50$, in addition to the $N = 28$ abundance peak, but also predict that this pattern does not persist over a large range of depths, therefore, not causing a significant conflict with observations. However, no experimental data exist for these nuclei. Masses, for example, determined with the time-of-flight technique at the HRS, are critical to understand whether there is an $N = 50$ abundance peak forming and to which depth it persists. The important nuclei are shown in Figure 1.9. Especially the nuclei with $N \leq 50$ are critical to determine which abundances get swept into the $N = 50$ peak (peak formation) and when, at higher neutron density, the composition breaks out towards lighter nuclei (peak destruction). As Figure 1.9 shows, FRIB400 will enable achieving this objective.

Recent work has also shown that for crusts formed from X-ray bursts, which produce very heavy ashes, there is a possibility for abundance to get trapped at dripline nuclei with $N = 82$. Unlike for the $N = 50$ case, current mass models predict here that this abundance peak persists to greater depth, therefore resulting in much slower cooling than observed for most sources. However, for one source, EXO 0748-676, model comparisons have indicated that a more impure crust may be needed to explain its somewhat slower than typical cooling [Deg14]. It has been proposed [Lau18] that this could be explained if an *rp* process in the bursts of this source produces heavier-than-typical nuclei, which form an $N = 82$ abundance peak in the crust. Nothing is known experimentally about the relevant nuclear masses and it is not possible to reliably predict whether such a peak would indeed be formed. Unlike for $N = 50$, the $N = 82$ abundance peak is produced from the heaviest tail end of the *rp*-process ashes, and everything is processed through a critical branch point at ^{104}Se ($Z = 34$). The key question is whether neutron captures transform ^{104}Se into $N = 82$ ^{116}Se as density increases, or whether electron capture and neutron emission proceed to lighter nuclei, avoiding the formation of an $N = 82$ peak. Again, this depends primarily on the nuclear masses of the Se isotopic chain out to ^{116}Se and the masses just below ^{104}Se. As

Figure 1.9 shows, measurements in this region require FRIB400. Finally, our knowledge of the masses of dripline nuclei is extremely limited. It is possible that structures in the mass surface, which affect the reaction sequence, emerge at unexpected locations. A mapping of the mass surface along the neutron dripline up to Se is, therefore, needed. The exciting prospect is that, as Figure 1.9 shows, this will be possible at FRIB400.
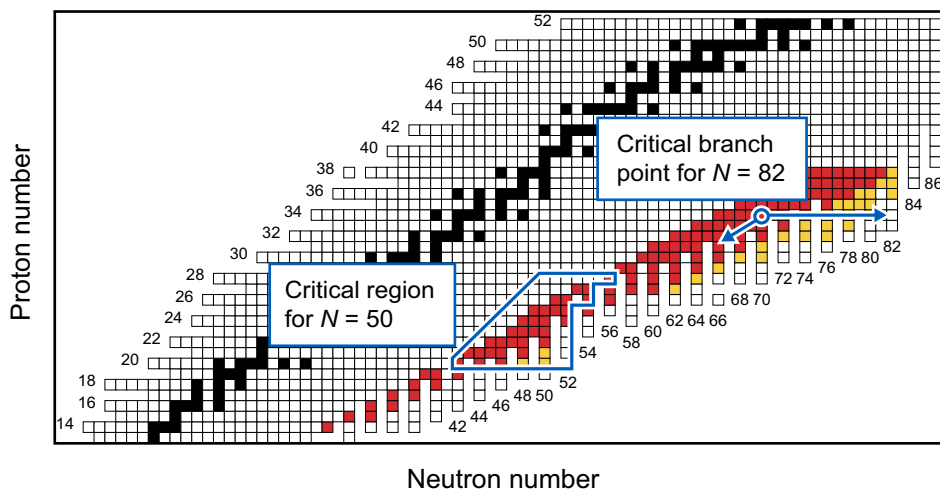
Figure 1.9: Chart of nuclides for which FRIB400 enables or significantly improves[1] mass measurements (red) and demonstration of neutron stability (yellow) for astrophysical purposes. Shown are only nuclides predicted to be neutron bound by the Finite Range Droplet Model (FRDM). The key regions for understanding neutron-star crust cooling based on current models are indicated.

In summary, the physics of neutron dripline nuclei is intimately connected with the cooling of transiently accreting neutron stars and needs to be understood to obtain constraints on dense matter from X-ray observations. FRIB400 offers increased rare-isotope production capabilities for nuclei in exactly the two key regions where they enable the experiments needed to address this problem.

1.4 FRIB400 and *r*-process nucleosynthesis

Identifying and understanding the astrophysical site of the formation of the heaviest elements via *r*-process nucleosynthesis is one of the foremost goals of nuclear astrophysics and is a primary science driver for FRIB [LRP15, NaD13, Apr18, Hor19, Cow19]. The recent observation of the neutron-star merger gravitational-wave event GW170817 and its associated kilonova provided a dramatic confirmation that at least some *r*-process elements can be made in such mergers. However, many open questions remain, including the nature of the nucleosynthetic sites within the merger and whether mergers can account for the galactic production of all *r*-process elements. Definitive answers require a reduction in the uncertainties entering *r*-process calculations, from astrophysics and from nuclear physics. On the nuclear physics side, only a fraction of the nuclear properties required for *r*-process

---

[1] Marked are nuclei for which the intensity gain from FRIB400 is at least a factor of two, for which FRIB400 intensities enable a measurement, and for which the 200 MeV/u intensities are insufficient for astrophysical purposes.

simulations, such as masses, half-lives, and neutron capture rates, are known. Hundreds of undiscovered nuclei will be accessible for the first time with FRIB, and FRIB400 will further extend the reach into key regions of the nuclear chart for *r*-process studies.

The emergence of neutron-star mergers as a likely site of the *r*-process highlights the need to study the most neutron-rich isotopes. FRIB400 will significantly extend the study of these isotopes.

The extended reach of FRIB400 for key *r*-process measurements is illustrated in Figure 1.10. Here, the mass and β-decay rate sensitivity-study results from the four distinct types of astrophysical conditions considered in [Mum16] are combined to highlight the region of the nuclear chart important for *r*-process simulations. This region extends from known data to the neutron dripline. Nuclei with significantly enhanced availability at FRIB400 are shown in color. FRIB400 will facilitate high-precision measurements on nuclei along the *r*-process path for all astrophysical conditions at the $N = 82$ and $N = 126$ closed shells; these nuclei are responsible for shaping the main abundance pattern features of the $A \sim 130$ and 195 peaks. FRIB400 will also provide access to the nuclei responsible for the rare-earth peak, a small abundance pattern feature between the $A \sim 130$ and 195 peaks, thought to form dynamically as the *r*-process path moves toward stability [Hor19]. Some nuclei relevant for the most neutron-rich *r*-process models will still be out of reach and
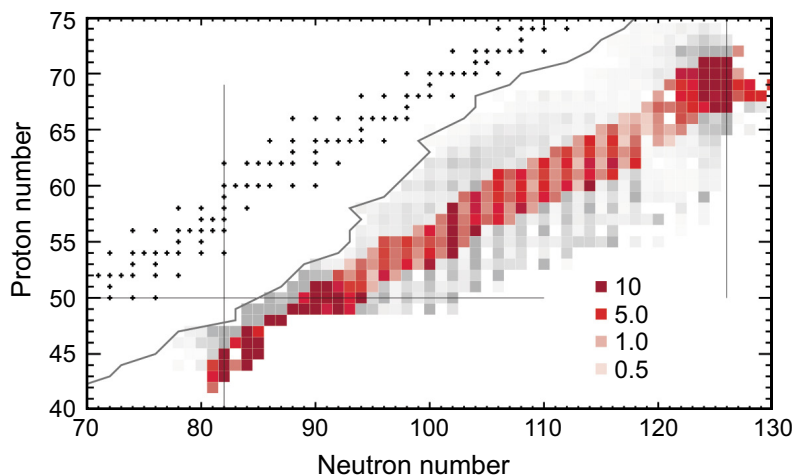
Figure 1.10: Combined sensitivity measures (the summed *r*-process abundance differences caused by the mass and β-decay half-life uncertainties) for mass and β-decay rate sensitivity studies run with four distinct types of astrophysical conditions: a high-entropy wind, a low-entropy wind, a cold wind, and cold neutron-star merger dynamical ejecta, from [Mum16]. Highlighted are nuclei where gains are expected with FRIB400 for astrophysical purposes. The sensitivity measures are shown in color for key nuclei that are anticipated to be more accessible with FRIB400 for β-decay and mass measurements[2]. For comparison, the gray line shows the extent of the Atomic Mass Evaluation 2016 (AME2016) [Wan17].

---

[2] For β-decay (mass) measurements, these are nuclei with rates of $> 10^{-5}$ ($> 10^{-4}$) with FRIB400—the minimum rate for such experiments—and with rates of less than 10^{-2} (less than 1) without the upgrade. Surpassing this second limit, increased precision would not have astrophysical impact anymore.

their properties will have to be predicted by theory. The increased reach with FRIB400 will be important to provide data that enable reliable predictions to extend into regions that will remain out of reach at any facility. The net result is that with the substantially reduced nuclear-physics uncertainties made possible with FRIB400, accurate modeling of abundance pattern features will become a sensitive probe of *r*-process conditions.

An example illustration of the reduction in abundance-pattern uncertainties anticipated with FRIB400 is given in Figure 1.11. The abundance-pattern bands shown are ranges that result from random, uncorrelated Monte-Carlo variations in nuclear masses assumed to be within the known uncertainties, which is large where experimental data is missing.
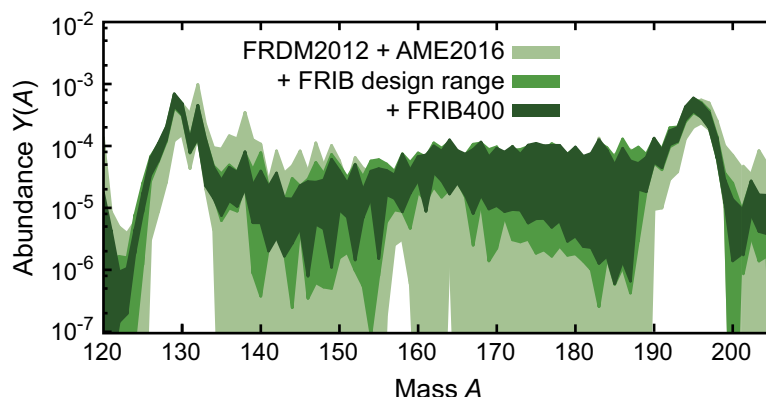
Figure 1.11: Ranges of abundance patterns produced from 5,000 sets of uncorrelated, random variations of individual nuclear masses outside the range of: the Atomic Mass Evaluation 2016 (light green band), the FRIB full power anticipated reach (green band), and the FRIB400 predicted reach (dark green band), for hot, low-entropy wind astrophysical conditions. Monte-Carlo *r*-process simulations were performed as described in [Sur18].

The astrophysical conditions used in these particular calculations are the ones of a low-entropy wind, similar to those expected for outflows from a neutron-star merger accretion disk [Sur16, Jus15, Mar15, Wan14, Sie17]. The simulations that make up the lightest band include variations of all masses outside the Atomic Mass Evaluation 2016 (AME2016), thus providing an indication of current uncertainties in *r*-process simulations due to unknown nuclear masses. It is clear that nuclear data uncertainties are currently too large to allow precision simulations of low-entropy wind nucleosynthesis. The medium and dark shaded bands show the range of patterns that result from variations of masses outside the anticipated FRIB and FRIB400 reach, respectively. FRIB400 holds the promise to significantly improve the reliability and precision of *r*-process simulations, for both the abundance-pattern matching as well as heating-rate calculations that are crucial for kilonova interpretation.

At FRIB400, the β-decay measurements can be performed with the FRIB Decay Station [FDS] and masses can be efficiently measured with the time-of-flight technique at the HRS [HRS].

Charge-exchange reactions and β-decay studies to constrain *r*-process models

An accurate knowledge of β-decay properties, nuclear level densities, and γ-strength functions is important for astrophysical processes in which β decays and (n,γ)/(γ,n) reactions play a role, including the (weak) *r* process and the *i* process [Mum16, Sur14, Den18]. Two novel and complementary techniques to constrain all of the above-mentioned nuclear inputs for one nucleus with a single experiment have been developed. One is the use of the inverse-kinematics (p,n) charge-exchange reaction in combination with the detection of in-flight γ rays in the Gamma-Ray Energy Tracking Array (GRETA) [Gre]. From the (p,n) charge-exchange reaction, the Gamow-Teller strength distribution can be extracted (see Section 3.1.2). This includes not only the strength within the limited β-decay Q-value window, but also strength at higher excitation energy, which is important for constraining models used to estimate the half-lives for large numbers of nuclei important for nucleosynthesis. Since the projectile-like (p,n) reaction residues are tagged in the HRS, including those that decay in flight by particle emission, neutron-emission probabilities are readily extracted. By tagging the γ-ray emission, nuclear level densities and γ-strength functions can be deduced with the Oslo approach [Spy14], accessing several relevant quantities in one experiment. The second technique is the use of total absorption spectroscopy to study the β-decay strength distribution, and to extract nuclear level densities and γ strength functions via the β-Oslo method [Spy14, Lid16]. While these studies are limited by the β-decay Q value, the advantage is that such measurements can be performed with much smaller beam intensities, down to approximately 1 particle per second. Both the charge-exchange reactions and the β-decay programs will benefit from FRIB400 (Sections 2.1 and 3.1.2).

Coulomb dissociation to constrain nucleosynthesis processes

Rare-isotope beams with energies available at FRIB400 open up the opportunity to use Coulomb dissociation to investigate astrophysical reaction rates for photo-disintegration and neutron-capture processes on short-lived radioactive nuclei that presently cannot be measured directly due to the lack of neutron or γ targets. In this technique, nuclei interact with the electric field of a heavy target nucleus, and the resulting quasi-real photons break up the nucleus. The power of this approach has been demonstrated, for example, with the proton-capture rate on ^{26}Si probed by Coulomb dissociation of ^{27}P at 400 MeV/u [Mar16] and the neutron-capture rate on ^{59}Fe probed by Coulomb dissociation of ^{60}Fe at 660 MeV/u [Ube14]. Neutron-capture rates on unstable nuclei play an important role in neutron-capture nucleosynthesis processes such as the rapid neutron-capture process. This r process is responsible for the origin of many of the heavy elements above iron, but all model predictions rely on theoretical reaction rates beyond the line of stability. These predictions require experimental confirmation. An example is the neutron-capture rate on ^{129}Cd in the r process that has been identified as one of the most important neutron-capture-rate sensitivities for r-process models [Sur18]. Coulomb dissociation of ^{130}Cd opens a pathway to constrain this reaction by studying the inverse of the capture reaction of interest. The optimum energy to achieve the required virtual photon spectrum by bombarding a lead target is around 400 MeV/u. In addition, photon induced nucleosynthesis patterns such as the p or γ process can also be directly studied. The quasi-real photon flux in Coulomb dissociation mimics the photon flux in supernova shock fronts that produces the so-called p-isotopes, stable neutron-deficient isotopes of elements beyond iron. The Coulomb-dissociation technique would allow for a direct study of many of the critical branching points in p-process nucleosynthesis environments. Examples are ^{110}Sn or ^{112}Xe, where (γ,n), (γ,p), and (γ,α) reactions compete. Measurements of the neutron channel require minimum beam energies above 250 MeV/u. The proton channel experiments would also strongly benefit from the energy upgrade as 400 MeV/u is close to the optimum energy.
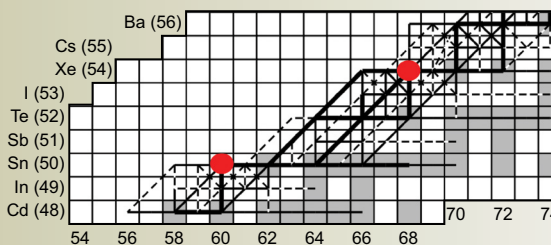
The picture, from [Rap06], shows the p-process reaction flows. Key branch points where multiple photon-induced reaction channels compete are readily identifiable. The two examples mentioned above, ^{110}Sn and ^{112}Xe, are marked.

2. Conquering new territories for nuclear structure studies

Two of the key challenges identified in the National Academies Decadal Study [NaD13] and the 2015 NSAC Long Range Plan [LRP15] for the field of nuclear science are: *"How does subatomic matter organize itself and what phenomena emerge?"* and *"What is the origin of visible matter?"* Answers to these compelling questions require measurements of properties of rare isotopes that provide important constraints for improving our understanding of the complex, difficult-to-model many-body forces at play—with the ultimate goal of a comprehensive description of all nuclei and their reactions with predictive power and quantified uncertainties [Naz16, Wes16]. Such rare isotopes will also quantify the role of the particle continuum that impacts all nuclear systems, including neutron stars.

For this purpose, nuclei in regions of the nuclear chart where rapid structural changes occur have emerged as key messengers to isolate the various effects at play. In Section 2.1, it is shown, with the example case of the $N = 50$ isotones below ^{78}Ni, how FRIB400 provides unprecedented access to such otherwise out-of-reach regions. Figure 2.1 illustrates the $N = 50$ isotonic chain of interest, so far largely located in terra incognita, where even the existence of most nuclei has not yet been established. Other territories of neutron-rich nuclei will benefit from a similarly dramatic increase in scientific reach from FRIB400 and are of similar importance. The cases presented here are representative of the gains that can be realized in other important regions of the nuclear chart.
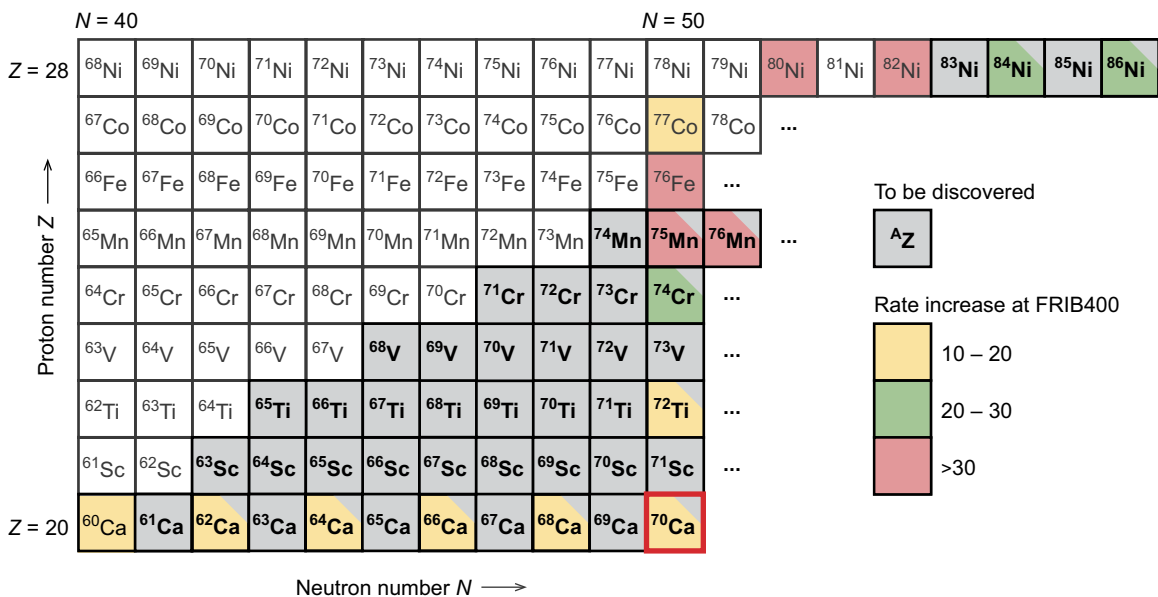
Figure 2.1: The territory of neutron-rich nuclei is arguably the most fertile ground for breakthroughs in nuclear structure research. The Ca-Ni region is of particular interest. This part of the nuclear chart shows the neutron-rich isotopes of $Z = 20$ Ca to $Z = 28$ Ni. Bold text and gray color indicate isotopes that have not yet been observed and, for selected example cases that will be discussed, color indicates the beam intensity gain afforded by FRIB400.

The nuclear landscape is delineated by the nucleon driplines [Erl12, Afa13]. They represent a fundamental benchmark for nuclear theory and pose important limits for astrophysical

processes. Along the $N = 50$ isotonic chain, the very neutron-rich nucleus ^{70}Ca with 50 neutrons and 20 protons (highlighted in Figure 2.1) is most likely the lightest bound $N = 50$ isotone and, in fact, is predicted to mark the neutron dripline in the magic calcium isotopic chain. In Section 2.2, the increased potential for isotope discovery with FRIB400 is demonstrated with the example of these Ca isotopes.

In the particle continuum, structural change is driven by weak binding and modified many-body correlations [For13]. Yet little-explored phenomena, such as two-neutron radioactivity or multi-neutron emission, will be encountered that allow for an unprecedented view on emergent phenomena such as clustering and pairing in the regime of weak binding. For extremely neutron-rich medium-mass nuclei, thick neutron skins are predicted to develop, offering, perhaps, an opportunity to study matter in the laboratory that is nearly as neutron-rich as that found in neutron stars. The access to extreme-skin nuclei in the Ni isotopic chain afforded by FRIB400 is laid out in Section 2.3.

2.1 Evolution of nuclear structure towards the dripline

In the quest for a predictive model of nuclei, experimental observables in regions of rapid structural evolution away from the valley of β stability are critical benchmarks for nuclear models as they point to the appropriate inclusion of the relevant degrees of freedom. In the history of nuclear structure physics, so-called islands of inversion have provided a wealth of insight, showcasing—in confined regions of the chart—the breakdown of shell gaps, the sudden onset of deformation and rapid shape changes, as well as the phenomenon of shape coexistence [Bro10, Hey11]. The newest addition to the group of islands of inversion is centered on ^{64}Cr ($N = 40$) [Len10], where some Cr and Fe nuclei are among the most deformed in the region in spite of the $N = 40$ subshell closure. A recent, exciting prediction extends this island to $N = 50$ [Now16], deep into nuclear terra incognita and including nuclei whose relevant properties can only be reached at FRIB400.

FRIB400 will enable the study of benchmark regions of the nuclear chart where rapid changes in the nuclear structure are expected.

The predictions have ^{78}Ni as being spherical (see also [Tan19]), ^{76}Fe as exhibiting triple shape-coexistence, and ^{74}Cr as being a well-deformed prolate rotor along the $N = 50$ isotonic chain [Now16]. The wealth of phenomena related to coexistence effects would be probed in experiments at FRIB through in-beam γ-ray and decay spectroscopy. Figure 2.2(a) provides the simulated γ-ray spectrum of ^{76}Fe as populated in a one-proton removal reaction and detected with GRETA [Gre] at the High Rigidity Spectrometer (HRS) [HRS] (top) at the nominal FRIB energy and (bottom) as performed at significantly increased luminosity with a thick liquid hydrogen target that is only afforded by FRIB400. FRIB400 would enable the first spectroscopy of this nucleus. In pursuit of information on collective degrees of freedom, inelastic proton scattering measurements are subject to comparable gains with the higher achievable beam energy at FRIB400, enabling such studies (see Figure 2.2(b)). For

^{74}Cr, first spectroscopy clearly will become possible only at FRIB400, as shown in Figure 2.2(c)—the comparable spectrum simulated at the nominal FRIB beam energy contained no events and is not shown. Further down the $N = 50$ isotonic chain, for ^{72}Ti, the β-decay half-life can be measured at FRIB400 with the FRIB Decay Station [FDS] to a precision of 30% in a typical implantation and decay experiment, while it would take 100 days to reach the same precision at the rates provided at the nominal FRIB beam energy. For the less exotic ^{74}Cr and ^{76}Fe nuclei, the β-decay half-lives can be measured with high precision after the upgrade due to the factors of 30 and 25 increase in the rate, respectively (see Figure 2.1). For ^{76}Fe, the population of excited states in the β decay of ^{76}Mn will become possible with statistics sufficient to characterize the predicted shape-coexisting excited 0^+ state (see Figure 2.2(c)) from its E0 strength, afforded by the factor of 30 increase in the beam intensity of the decay parent ^{76}Mn. With the above-mentioned key measurements, this exciting region of the nuclear chart could be explored with FRIB400 while remaining out of reach at the nominal FRIB beam energy. The most neutron-rich $N = 50$ isotone predicted to possibly exist is ^{70}Ca [Neu19] and this nucleus is the subject of the next section.
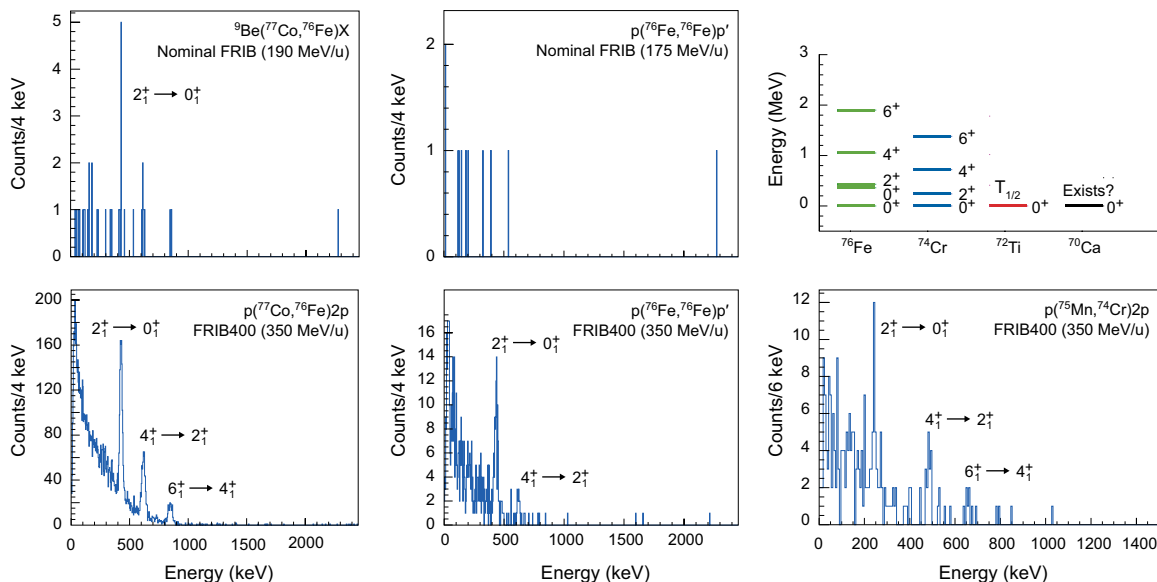
Figure 2.2(a): Simulated γ-ray spectra for the one-proton removal to ^{76}Fe measured with the Gamma-Ray Energy Tracking Array (GRETA) at the High Rigidity Spectrometer (HRS) for the nominal FRIB beam energy (top) and at FRIB400 using a MINOS-type target (bottom). A typical 100-hour measurement is assumed.

Figure 2.2(b): Simulated γ-ray spectra for the inelastic proton scattering of ^{76}Fe measured with GRETA at the HRS for the nominal FRIB beam energy (top) and at FRIB400 using a MINOS-type target (bottom), under the assumption of a 72-hour run.

Figure 2.2(c): Predicted level schemes [Now16] of the nuclei of interest with the states reachable with FRIB400 indicated (top). Simulated γ-ray spectra for the one-proton removal to ^{74}Cr at FRIB400 using a MINOS-type target with GRETA at the HRS (bottom). This experiment would require 200 hours of beam on target.

The gains that enable the measurement techniques sketched above are related to various aspects of FRIB400: (i) the increase in projectile rate in the case of reactions or the increase in rate of the parent nucleus in β-decay studies, and (ii) for reactions, the energy upgrade

offers—starting at about 300 MeV/u—the opportunity to use a very thick liquid hydrogen target, affording an unmatched luminosity gain on top of the increased projectile rates. More background on such a thick liquid hydrogen target is given in the sidebar.

Maximizing luminosity for the rarest isotopes

FRIB400 offers the possibility to push in-beam spectroscopy measurements even further toward the limits of existence, with the use of thick targets enabled by the higher beam energy, allowing increased luminosity for direct reactions, such as proton removal, to populate and study the most exotic nuclei. Anticipated as a key instrument for such studies, GRETA, covering approximately 80% of the full 4π solid angle with high-resolution HPGe, will provide a world-unique capability to detect and track γ rays with unprecedented efficiency, background rejection, and energy and position resolution at FRIB. However, in order to maintain good energy resolution, it is often necessary to limit the target thickness, which in turn limits the experimental sensitivity. The target considerations to optimize experiment statistics and sensitivity are in direct conflict—thicker targets, providing the desired luminosity increase, introduce uncertainty in the position at which a reaction occurs and for the velocity at γ-ray emission, limiting the resolving power with reduced resolution as a result of Doppler broadening.

However, this challenge can and will be addressed with the development of a thick cryogenic target and vertex tracking detector system for GRETA at FRIB, modeled after the MINOS (MagIc Numbers Off Stability) system developed at CEA-Saclay [Obe14]. A thick cryogenic target, of order 10-15 cm in thickness, will be combined with a multi-layer barrel-geometry tracking detector system, able to detect protons scattered in (p,2p) or similar reactions and enabling reconstruction of the reaction vertex depth in the target with mm resolution. At FRIB400, this will enable high-luminosity, thick-target measurements while maintaining an effective γ-ray resolution of order of 2%, as compared to the 12-15% for a corresponding measurement with solid C or Be targets. The gains in γ-ray yield through the increased luminosity are illustrated in the simulated spectra displayed in Figure 2.2(a-c).

2.2 Opportunities for isotope discovery—exploring the limits of existence for key isotopes

The nuclear chart is bounded by the nucleon driplines. They represent a fundamental benchmark for the modeling of nuclear binding, and they provide important limits for astrophysical processes in a variety of nucleosynthesis scenarios. While the proton dripline has been identified for many elements, the neutron dripline has not been established past $Z = 10$ (neon). FRIB will facilitate far-reaching exploration of the neutron dripline beyond neon and may reach the dripline in places up to $Z = 30$. However, given recent results from RIKEN on the location of the dripline [Tar18], FRIB400 will be needed to reach most of the dripline up to $Z = 60$. In particular, semi-magic chains such as Ca, Ni and Sn should be viewed as key benchmarks, arguably the most critical ones to look at from a theory perspective, because they provide a golden opportunity to create a bridge between the refined methods based on realistic interactions, in which all A nucleons are considered as elementary degrees of freedom, and configuration-interaction models based on the concept of valence

nucleons, as well as nuclear density functional theory describing nuclei in terms of proton and neutron local densities and currents. Predicting the outlines of the entire nuclear chart is in the realm of density functional theory, which has advanced to employ Bayesian approaches for uncertainty quantification of extrapolated observables [Neu18].

FRIB400 will double the number of elements from atomic number 30 to 60 for which the neutron dripline will be in reach.

Figure 2.3 presents the calculated probability of existence for the Ca to Ni isotopic chains from $N = 40$ to $N = 60$. For calcium, ^{70}Ca with $N = 50$ is expected to be the last neutron-bound isotope with a probability of existence exceeding 50%. Indeed, the figure indicates that the neutron dripline proceeds very far from stability and likely extends to ^{70}Ca. The recent observation of ^{60}Ca [Tar18] indicates that the approaches used in Figure 2.3 are likely more accurate than some early ab-initio-type theories that predicted the dripline at ^{60}Ca. A consequence is that the dripline is further from stability than was previously expected—now also supported by new many-body calculations based on chiral NN and NNN forces [Hol19]. While ^{60}Ca was only discovered recently, it is predicted that FRIB at the nominal beam energy would have a significantly expanded reach and produce more than 10 ^{64}Ca nuclides per week in a discovery experiment that uses the fragmentation of a ^{82}Se primary beam. Within the same experimental framework, ^{66}Ca would constitute the limit for isotope discovery with 1 event per week. With FRIB400, ^{68}Ca production is predicted to be feasible with about 1 event per week, further pushing out the frontier for isotope discovery. The gains here lie in the improved transmission of the fragmentation products and—through the use of thicker production targets—the increased probability for secondary reactions within the thick target. For the case of ^{70}Ca, it is plausible that it could be produced at FRIB400 at a rate of 1 event per 2 weeks from a uranium beam, involving abrasion to a low-excited fissile nucleus and subsequent two-step fragmentation after fission. Moreover, the full reach along the dripline made possible by FRIB400 could extend to $Z = 60$ and to the $N = 126$ shell closure as shown in Figure 2.4. This would, however, require production target developments in addition to the energy upgrade to realize the full gain.

Z\N	40	41	42	43	44	45	46	47	48	49	50	51	52	53	54	55	56	57	58	59	60
Ni	100.0	100.0	100.0	100.0	100.0	100.0	100.0	100.0	100.0	100.0	100.0	99.9	100.0	97.4	100.0	88.4	99.9	70.9	99.3	44.8	92.1
Co	100.0	100.0	100.0	100.0	100.0	100.0	100.0	100.0	100.0	100.0	100.0	98.7	100.0	94.6	100.0	83.7	99.9	64.8	97.1	36.1	79.8
Fe	100.0	100.0	100.0	100.0	100.0	100.0	100.0	100.0	100.0	99.9	100.0	92.6	99.9	77.1	99.6	67.3	95.1	52.0	88.8	25.4	67.9
Mn	100.0	100.0	100.0	100.0	100.0	100.0	100.0	99.9	100.0	98.5	100.0	85.4	99.8	63.1	97.3	56.2	88.0	40.5	78.2	16.5	58.0
Cr	100.0	100.0	100.0	100.0	100.0	99.9	100.0	98.3	100.0	90.1	100.0	56.6	98.4	39.0	84.3	35.8	77.1	26.8	68.3	10.5	45.6
V	100.0	100.0	100.0	99.8	100.0	98.8	100.0	91.8	100.0	74.0	99.9	38.9	91.5	26.0	78.3	24.1	73.0	15.6	61.9	4.5	35.2
Ti	100.0	97.6	100.0	91.8	100.0	85.6	100.0	65.8	99.6	39.5	96.4	18.8	73.6	14.4	63.3	14.4	60.8	8.7	46.9	2.8	24.8
Sc	100.0	87.0	100.0	64.5	99.9	55.5	99.6	36.5	97.7	22.3	89.3	9.1	63.5	6.4	53.8	6.5	50.0	2.9	33.5	0.8	15.7
Ca	100.0	45.7	98.3	21.2	88.8	12.7	81.9	10.2	75.8	5.8	56.8	4.1	45.1	3.4	39.5	3.5	35.7	1.6	22.5	0.5	11.1

Figure 2.3: Calculated probability of existence in percent for the Ca to Ni isotopic chains from $N = 40$ to $N = 60$ deduced from Bayesian model mixing employing density functional theory and Gaussian processes [Neu18]. Green represents a high probability the isotope is bound, while red indicates a low probability. The nucleus ^{70}Ca is the most neutron-laden $Z = 20$ isotope predicted to exist with more than 50% probability [Neu19].

At the heart of rare-isotope science, and what distinguishes rare isotopes from their stable cousins, is the proximity of the particle continuum where open-system phenomena alter

nuclear structure as compared to observations in well-bound nuclei [For13, Hag13]. For calcium, the odd-mass isotopes starting with ^{61}Ca are already predicted to have probabilities of existence below 50% [Neu19]. These nuclei are very interesting for studies with invariant mass spectroscopy where the energetics of the unbound ground and excited states are reconstructed from the 4-momentum vectors of the decay products measured, for example, at the HRS with neutron detection. Data on their level schemes will be invaluable for the exploration of continuum effects and correlations near or above the particle-decay thresholds [Dob07]. Such data are critical to test the inclusion of weak-binding effects in every class of nuclear models, and will enable the exploration of new phenomena [Hag13] such as two-neutron radioactivity and di-neutron decay. The increase in reach for the odd-mass Ca isotopes mirrors that for the even-mass ones quantified above. At FRIB, neutron-unbound excited states in the recently discovered nucleus ^{59}Ca [Tar18] will be within reach, while at FRIB400, depending on the existence of the $N = 41$ isotones of Sc and Ti, the predicted neutron-unbound ground and excited states of ^{61}Ca will be accessible with invariant mass spectroscopy at the HRS in one- or two-proton removal reactions using a thick liquid hydrogen target. This may well be the only unbound Ca isotope accessible for neutron spectroscopy.
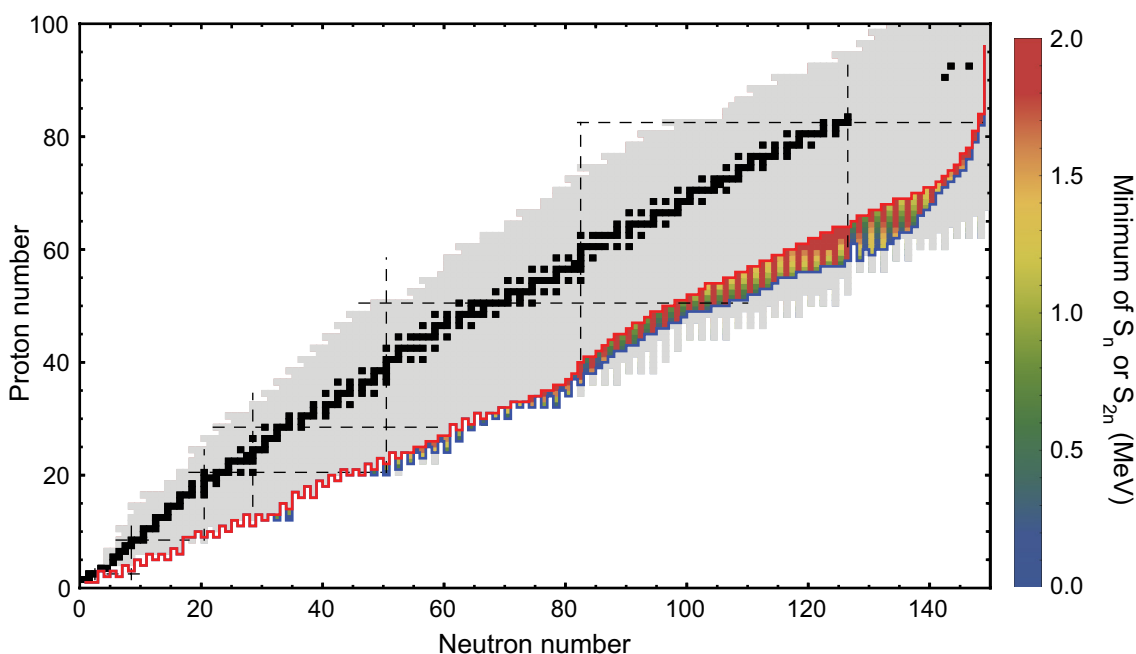
Figure 2.4: Increased reach for isotope-discovery experiments (1 atom per week) at FRIB400. Nuclei predicted to exist according to UNEDF0 energy density functional calculations are indicated in gray. The reach with FRIB for isotope discovery is marked by the red line. The blue line shows the significantly increased reach for isotope-discovery experiments with FRIB400. The region in between these two limits is color coded according to the predicted minimum neutron separation energy, offering a wide territory to explore phenomena in the regime of weak binding. The increased production of neutron-rich heavy nuclei will allow reaching the dripline up to $Z = 60$ with FRIB400 as compared to $Z = 30$ at nominal FRIB beam energies.

Figure 2.4 shows the significant increase in the potential for isotope discovery with FRIB400. The production of neutron-rich medium-heavy and heavy nuclei is greatly enhanced and will allow reaching the neutron dripline up to $Z = 60$ with FRIB400 as

compared to $Z = 30$ at FRIB. At and beyond the proton dripline, the advantage is not as much the increased beam intensity but rather the significant improvements in beam purity, for example, reducing the contaminants for a beam of ^{100}Sn by a factor of 1,000 (see also Section 5.4). This would open up broad programs that explore (multiple) proton emission and correlation effects in proton unbound medium-mass and heavy nuclei.

2.3 Phenomena in the regime of weak binding—nuclei with extreme neutron skins come within reach

At the dawn of rare-isotope science, neutron halo nuclei [Tan85, Han87, Oza01] represented a frontier for exotic phenomena to be studied at first-generation rare-isotope facilities. The halo is a threshold effect that arises, in light nuclei, from the very weak binding of the outermost neutrons. At FRIB, very neutron-rich medium-heavy nuclei will be within reach for which the excess neutrons are predicted to form a skin surrounding a core, i.e. the neutron distribution will reach beyond the proton one. Neutron-skin thickness is a unique indicator of the isovector properties of atomic nuclei, and it correlates strongly with observables that depend on the nuclear symmetry energy that characterizes the nuclear
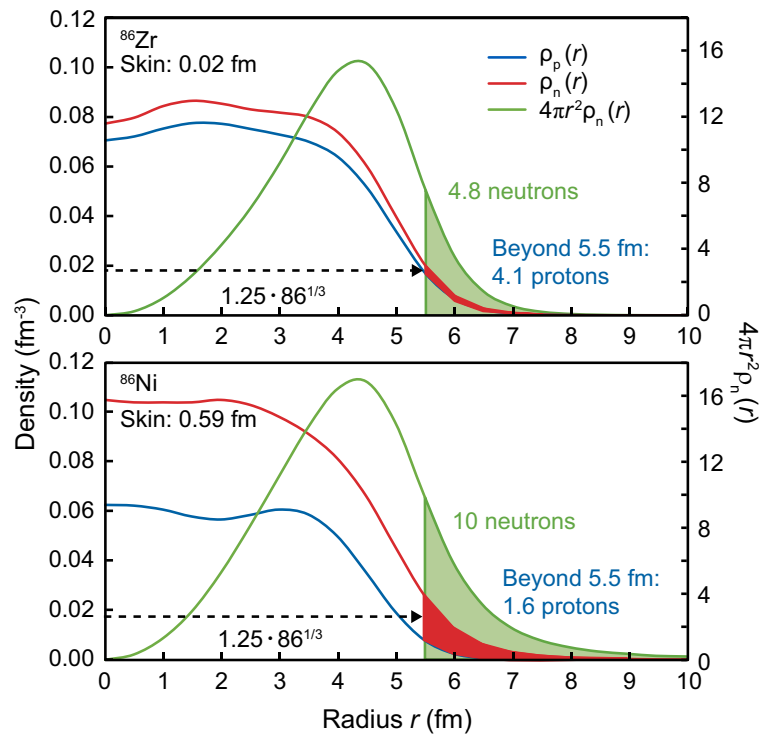
Figure 2.5: Radial proton (blue) and neutron (red) densities as well as the expected number of neutrons at a given radius, r, in ^{86}Zr (top) and ^{86}Ni (bottom). The red area highlights the neutron excess in the surface beyond 5.5 fm. The green shaded area corresponds to the number of neutrons beyond 5.5 fm, amounting to 4.8 in Zr and 10 in Ni. This underlines the unique nuclear surface to be encountered in ^{86}Ni, rivaled in neutron richness perhaps only by neutron stars. Reactions performed with extreme-skin nuclei will allow to explore some of the most neutron-rich matter available in the laboratory. Densities are taken from SkX Skyrme [Bro98] HF calculations—other functionals such as UNEDF1 [FME, Kor13] predict very similar neutron skin thicknesses.

matter equation of state [Bro00, Fur02, Rei10] at low density (see Section 1.1). The most neutron-rich nuclei of the Ni isotopic chain, e.g. ^{84,86}Ni, have long been predicted to exhibit extreme neutron skins, offering unique laboratories to study the most neutron-rich matter available in the laboratory through reactions and scattering experiments. At FRIB with the nominal beam energy, ^{84}Ni, with a predicted 0.5-fm neutron skin, will be in reach for pioneering reaction and interaction cross section measurements at the HRS.

FRIB400 will enable study of very neutron-rich nuclei such as ^{86}Ni, predicted to have an extreme neutron skin.

At FRIB400, the factor of 20 increase in the rate of ^{84,86}Ni will enable (i) basic scattering studies to probe, in the laboratory, such very neutron-rich matter as found in the surface of the extreme-skin nucleus ^{86}Ni, and (ii) enable first precision studies of ^{84}Ni via a variety of reactions (e.g. see Section 3.1.3). As outlined in Section 3, the higher available beam energy actually improves the validity of approximations used in the typical models describing reactions with fast beams, thus placing the experiments aimed at probing skins on a more solid footing.

The very neutron-rich ^{86}Ni is predicted to have an almost 0.6-fm thick neutron skin in stark contrast to its isobar ^{86}Zr whose slight neutron excess results in a 0.02-fm neutron skin. Figure 2.5 shows the radial proton and neutron density distributions of ^{86}Zr and ^{86}Ni and the corresponding expected number of neutrons at a given radius r. To highlight the stark difference in the surfaces of ^{86}Zr and ^{86}Ni, the neutron density extending beyond the proton density is indicated in red past a radius of $1 \cdot 25 \, A^{1/3} = 5.5$ fm. For illustration purposes, beyond 5.5 fm, the neutron-to-proton ratio is $4.8/4.1 \sim 1$ in ^{86}Zr and $10/1.6 > 6$ in ^{86}Ni, approaching the neutron-to-proton ratio expected in neutron stars.

3. Advancing nuclear reactions at FRIB400

Nuclear reactions are versatile tools used to explore the structure of nuclei, probe correlation effects, constrain the nuclear-matter equation of state, study electroweak interactions, and recreate processes that are relevant for nucleosynthesis in the Universe or for the nation's stockpile stewardship mission. They play a central role in addressing essentially all of the challenges put forth in the National Academies Decadal Study [NaD13] and the 2015 NSAC Long Range Plan [LRP15] for the field of low-energy nuclear science. Depending on the reaction mechanism to be employed and the degrees of freedom to be probed, the required beam energies vary from keV/u to GeV/u. Particularly useful for very weak beams of rare isotopes are reactions induced at high energies, around and exceeding 100 MeV/u, where kinematic forward focusing enables large-acceptance measurements and thick targets allow for a restored luminosity at low beam intensity. Figure 3.1 illustrates, schematically, the range of nuclear reaction mechanisms as a function of energy. The low-energy region is covered by reaccelerated beams and the intermediate range, to about 200 MeV/u, is covered by the nominal FRIB beam energy. To use the full spectrum, an upgrade to FRIB400 is required. The reaction program possible with FRIB400 is outlined in the following sections.
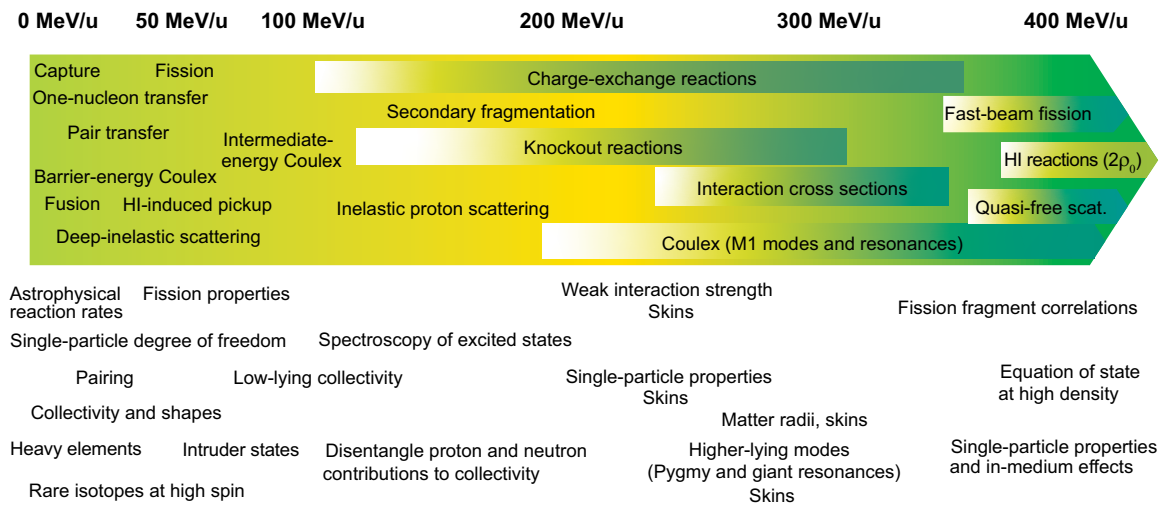
Figure 3.1: Reaction energy and the associated physics interest, relevant for nuclear structure physics, astrophysics, and applications. The desired energy range for the specific application of the reaction is indicated. The methods beyond 200 MeV/u are discussed here.

Another important consideration is that, to extract nuclear structure information, reaction theories are often required, which, in the high-energy regime of small scattering angles and short interaction times, can be formulated in the framework of Glauber multiple-scattering theory in the optical limit using the eikonal and sudden approximations, herewith avoiding uncertain (or unknown) optical model potentials. FRIB400 would (i) minimize distortions in the energy-dependent nucleon-nucleon (*NN*) cross sections input to the majority of fast-beam reaction models, (ii) transform the study of fission due to kinematic focusing, and (iii) open up the exploration of certain excitation modes and phenomena as energy thresholds are overcome (pion production) and strongly energy-dependent cross sections are enhanced.

3.1 Exploiting the energy dependence of free nucleon-nucleon cross sections—minimizing distortions

A strength of fast-beam reactions is that, for their interpretation, free *NN* cross sections can often be used. The energy dependence of these illustrates the inherent advantage of the 400 MeV/u energy upgrade of FRIB. The *NN* cross section is minimized and relatively flat between 200 and 500 MeV (see Figure 3.2), driven by the rapid decrease of the central isoscalar component approaching 200 MeV (see Figure 3.3), making the nucleus more transparent, minimizing distortions, and reducing final-state interactions. This reduces the uncertainty in the extraction of nuclear structure or nuclear astrophysics information from any reaction theory that relies on *NN* cross sections in the energy regime from 200 to 500 MeV/u.
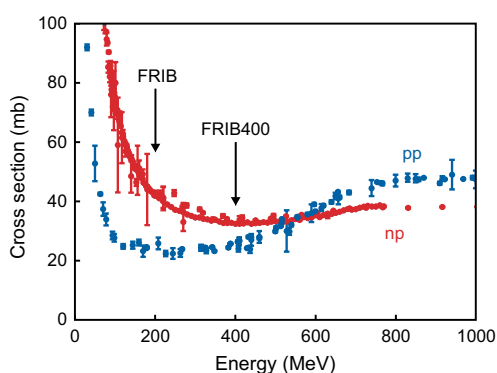
Figure 3.2: Nucleon-nucleon (*NN*) cross sections as a function of energy (data from [Tan18]). At energies close to 400 MeV, the *NN* cross sections are minimized and the nucleus becomes most transparent.
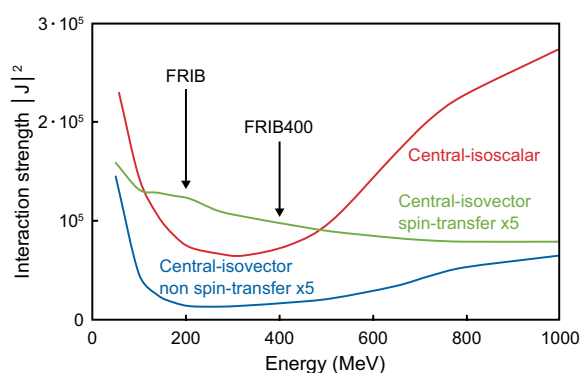
Figure 3.3: *NN* interaction strengths projected on central-isoscalar, central-isovector spin-transfer, and central-isovector non spin-transfer components based on [Fra85]. At FRIB400, reactions can be interpreted with minimized distortion effects.

3.1.1 Quasi-free scattering—a new probe comes into reach

Inverse-kinematics quasi-free (p,p*N*) reactions are powerful probes complementing transfer, HI-induced knockout, and Coulomb-breakup reactions for studying nuclear wave functions of rare isotopes. In contrast to the other probes that are surface-dominated, quasi-free scattering accesses the interior of the nucleus. Therefore, complete spectral functions of protons and neutrons, ranging from deeply-bound to valence, can be extracted on an equal footing. As can be seen from Figure 3.2, the nucleus is most transparent around 200 to 400 MeV/u, making this an important energy range. Related, inverse-kinematics two-nucleon removal reactions on rare isotopes will add important information to the body of electron scattering data on stable nuclei. The latter have been interpreted to indicate that 20% of the nucleons in nuclei are engaged in short-range correlated pairs in the high-momentum tail of the nuclear momentum distribution, with such correlated nucleons being dominated by p-n pairs [Hen17]. There is evidence that the number of protons engaged in short-range correlated pairs increases in neutron-rich stable nuclei [Due18], prompting questions about how this observation will develop further in very isospin-asymmetric systems, beyond the valley of stability, and what the impact will be on nuclear models

that use low-momentum cut-offs in the renormalization procedures that soften the input interactions. In the foreseeable future, (p,pN) and (p,p2N) reactions will be the best tool to complement the studies pioneered with electron-induced reactions for rare isotopes with extreme values of N/Z within the energy regime that is relevant for nuclear forces in nuclei. The conditions of nuclear quasi-free reactions at around 300 to 400 MeV/u are the best match to electron quasi-elastic scattering data.

FRIB400 will enable quasi-free knockout reactions to be used in the regime where nuclei are most transparent and distortions and final-state interactions are minimized.

A complication of these measurements is that, since (p,pN) is a penetrating probe, in-medium effects and re-scattering have to be well understood for a quantitative analysis [Kre95, Hat97, Cow98, Aum13]. FRIB400 will make this possible and open the use of quasi-free scattering to probe rare isotopes. To reduce distortion effects and final-state interactions, it is important that such reactions be performed at an energy where the central isoscalar component of the NN interaction is minimal for both the incoming and outgoing channel [Aum13]. As seen in Figure 3.2, this is accomplished when the two protons in a (p,2p) reaction, for example, carry 200 to 250 MeV each in an equal sharing scenario, corresponding to a rare-isotope beam energy of 400 to 500 MeV/u. Indeed, the first inverse-kinematics (p,pN) measurements with rare-isotope projectile beams have been performed at 350 to 400 MeV/u [Pan16, Ata18, Dia18]. At nominal FRIB beam energies below 200 MeV/u, the protons in the entrance and exit channels would have energies of 100 MeV or less and, hence, coincide with the steepest region of the energy dependence of the NN interaction, making an analysis more uncertain.

Another advantage of the higher energy is that it enables application of (p,pN) reactions for γ-ray spectroscopy purposes. The use of a liquid hydrogen target, with the tracking capability of the MINOS-type [Obe14], would have a significant luminosity advantage as highlighted in the sidebar to Section 2.1. Additionally, the higher energy would make possible study of cluster knockouts, such as (p,pd) and (p,pα), as well as of nucleon-nucleon correlations and of cluster structures in nuclei.

3.1.2 Advancing charge-exchange reactions

The investigation of the spin-isospin response of nuclei through charge-exchange reactions at sufficient energy is a well-established technique that has important applications in nuclear astrophysics [Lan03] (see also Sections 1.3 and 1.4). For example, the indirect extraction of Gamow-Teller transition strengths [Tad87] at excitation energies inaccessible through β-decay studies has been particularly impactful. Aside from astrophysical motivations, there are significant scientific opportunities with (p,n) charge-exchange experiments in inverse kinematics [Sas11, Sas12] associated with fundamental properties of nuclei. These include the study of the quenching of the axial vector coupling constant g_A in nuclei [Suh17] and efforts to test the operator used to calculate matrix elements for neutrino-less

double β decay [Eng17, Cir18]. FRIB400 will reduce the systematic uncertainties in the extraction of the weak-interaction strength associated with the charge-exchange reaction mechanism. Essentially all quantitative analyses of charge-exchange reactions rely on the well-established proportionality between Gamow-Teller strength and the charge-exchange cross section at small momentum transfer [Tad87]. A lower limit of about 100 MeV/u is imposed by the need to minimize the contribution from multi-step processes and maintain the validity of the above-mentioned proportionality. As illustrated in Figure 3.3, the central isovector spin-transfer component of the *NN* interaction only has a weak dependence on energy and imposes no energy limitations. Owing to the strong reduction of the central-isoscalar component of the *NN* interaction (Figure 3.3, red), the distortions in the entrance and exit channels are significantly reduced between 200 and 400 MeV/u. In addition, the contributions to the charge-exchange cross section mediated by the central-isovector non-spin-transfer component of the *NN* interaction (Figure 3.3, blue) are strongly suppressed. At FRIB400, such measurements could be performed at the HRS with auxiliary neutron, light charged-particle, and γ-ray detection. In addition to electron-capture rates, charge-exchange reactions are key to a number of important parameters needed to model processes mediated by the weak force. Two examples are given in the following subsections.

FRIB400 will reduce systematic uncertainties in the extraction of weak interaction strength.

3.1.2.1 Gamow-Teller strength

The study of isovector excitations through charge-exchange reactions at intermediate energies is an important tool for exploring the spin-isospin response of nuclei [Ost92, Har01]. Of particular interest for testing nuclear structure models using charge-exchange reactions is the study of Gamow-Teller (GT) excitations. GT transition strength can be extracted from such experiments at excitation energies outside of the Q-value window accessible in β decay, including the GT giant-resonance region. GT strength distributions are very sensitive to the shell structure of the nucleus being probed, and experiments are particularly interesting in regions where the structure changes rapidly or is unknown. Charge-exchange experiments at the HRS with decay particle detection will allow to pinpoint the particle-hole content of GT strength and, in doing so, inform on the underlying configurations. Analyses typically involve a multipole decomposition and Figure 3.4 demonstrates one of the advantages of FRIB400. The isobaric analog state, which is a Fermi transition with no spin transfer and thus is not a part of the GT strength, is strongly reduced at 300 MeV/u as compared to 115 MeV/u. This is due to the diminishing central isovector non-spin transfer component of the *NN* interaction with energy, as seen in Figure 3.3. Hence, FRIB400 will reduce the systematic uncertainties associated with the reaction mechanism in the extraction of the weak-interaction strength from charge-exchange reactions.

An interesting candidate for the study of the quenching of the axial vector coupling constant g_A is the doubly-magic nucleus ^{24}O. This quenching of g_A is apparent in the over-prediction of β-decay matrix elements when using the bare value of g_A. Similarly, in charge-exchange experiments, only about 50-60% of the GT sum-rule strength is observed at excitation energies up to the giant-resonance region (below ~20 MeV) [Gaa81, Gaa85]. This quenching has been attributed to limited model spaces, missing two-body currents, and missing couplings to hadronic excitations in the theory and remains a subject of debate [Suh17]. In any case, it is important to test model predictions for the distribution of GT strength within the assumptions of any structure model. The field only now begins to understand and model mechanisms responsible for the long-standing quenching issue [Gys19] that has important implications for neutrino physics and astrophysics. For a system as neutron-rich as ^{24}O, GT transitions in the $β^+$ direction are completely Pauli blocked and the GT strength dominates the response, even up to high excitation energies, such as shown for $^{16}C(p,n)$ [Lip18] in Figure 3.4. With a (p,n) reaction at the HRS, the total strength and particle-hole composition of the GT resonance can be pinned down and serve as a benchmark for theory in the quest to disentangle the contributions to the quenching of g_A. The high intensity of a ^{24}O beam at FRIB400 makes a detailed study of GT strength possible.
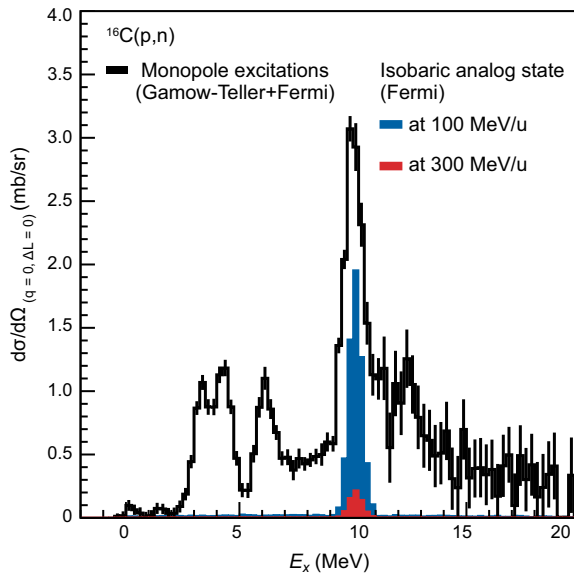
Figure 3.4: Extracted monopole cross sections at zero momentum transfer from the $^{16}C(p,n)$ reaction at 115 MeV/u [Lip18]. The monopole cross sections are due to contributions from Gamow-Teller (with spin transfer) and Fermi (no spin transfer) excitations. The estimated contribution from the latter, which is contained within the isobaric analog state (IAS), has to be subtracted to create the response from Gamow-Teller excitations only. At 115 MeV/u, the excitation of the isobaric analog state is strong. At 300 MeV/u, possible with FRIB400, the excitation of the IAS is reduced by about an order of magnitude.

3.1.2.2 Determination of the Landau-Migdal coupling constant

The interaction between proton particles and neutron holes in the $J^\pi = 1^+$ spin-isospin channel gives rise to a giant charge-exchange resonance in all nuclei with excess neutrons. The spin-isospin channel of effective interactions and energy density functionals can be characterized by the Landau-Migdal coupling constant g'_0 [Ost92] that is sensitive to the location, shape, and strengths of the Gamow-Teller (GT) resonance (see Figure 3.5). Global models based on density functional theory and the random phase approximation (RPA) require a calibration of g'_0 to provide reasonable β-decay properties, important, for example, for

r-process modeling or two-neutrino and neutrino-less double β-decay calculations [Mus16]. In general, the ability to model GT resonances is crucial for predictions of nuclear β decay.
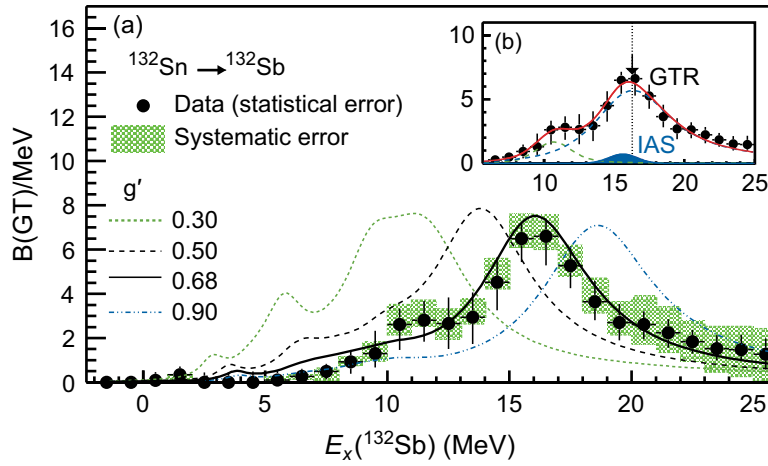
Figure 3.5: (a) Gamow-Teller resonance (GTR) extracted from the ^{132}Sn(p,n) reaction and comparison with theoretical calculation in which the Landau-Migdal parameter g_0' is varied to best match the data (black line). (b) Estimated contribution from the isobaric analog state (IAS) to the extracted strength distribution. Owing to strong suppression of the non-spin-transfer strength at beam energies in excess of 200 MeV/u, this contribution is very small (figure adapted with permission from [Yas18]).

In terms of nuclear matter properties, g_0' can also be interpreted as a measure of the interactions that may cause pion condensation [Mig78, Mey81], a phase transition that could occur in dense nuclear matter such as in the interior of neutron stars. Since the peak location of the GT resonance is strongly correlated with g_0', high-precision measurements of this GT resonance in nuclei with large neutron excess provide insight into the evolution of g_0' as a function of isospin asymmetry. As exemplified by the recent measurement of the GT resonance in the ^{132}Sn(p,n) reaction at 220 MeV/u [Yas18] (see Figure 3.5), it has become possible to extract the peak and width of the GT resonance for transitions from rare isotopes at beam intensities as low as 10^4 particles per second with a quality comparable to that achieved for stable nuclei. The extracted value for g_0' is within error bars equal to that of ^{208}Pb [Yas18]. It will be important to expand such measurements to very asymmetric systems, including those along isotopic chains. These experiments are possible with FRIB400, for example, from ^{180}Pb to ^{220}Pb and from ^{36}Ca to ^{52}Ca. The reduced uncertainties at high beam energies for the extraction of the GT strength through a multipole decomposition analysis are associated with the minimization of the distortions caused by the central-isoscalar component of the *NN* interaction. Together with the ability to use a thick liquid hydrogen target, this approach benefits from (p,n) experiments in inverse kinematics. Therefore, FRIB400 will result in opportunities to extract high-quality information about g_0' for very neutron-rich systems.

3.1.3 Exploring neutron skins and radii through cross-section measurements

As described in Section 2.3, the exploration of very neutron-rich medium-heavy nuclei with thick neutron skins will be within reach at FRIB400 (see Figure 2.4). Measurements of the neutron skin thickness offer constraints on the equation of state of nuclear matter near/ below saturation density [Fat18, Li14] (see Section 1.1). One way to deduce the neutron skin thickness is from the *rms* radii of matter and proton distributions. Proton radii are deduced from charge radii, which are often determined with the help of precision atomic-physics techniques involving laser spectroscopy schemes accompanied by demanding atomic-physics calculations of many-electron systems. At FRIB400, matter radii can be determined from reaction and interaction cross section measurements [Tan85, Han87, Oza01] with Glauber theory. Charge-changing cross sections will allow extraction of charge radii [Yam11, Est14] on a similar footing and for beams not intense enough for laser spectroscopy. Aside from skins, the evolution of charge radii along an isotopic chain can display signatures of shell closures, of pairing correlations, and of continuum effects [Ang13, Rui16, Mil19].

FRIB400 will improve the accuracy for the determination of key nuclear quantities such as the thickness of neutron skins.

Measurements of the reaction/interaction and charge-changing cross sections need to be carried out with uncertainties of less than 1% for the determination of neutron-skin thicknesses with a required accuracy of less than 0.05 fm in the case of medium-heavy nuclei and with uncertainties of 1 to 2% for information on the evolution of structure along an isotopic chain. This will be possible with FRIB400. The reduction of uncertainties introduced by the reliance on Glauber theory and its input free *NN* cross sections to the necessary level requires that the effects of distortions be minimized. As discussed above, this is best accomplished with experiments performed at beam energies exceeding 300 MeV/u, where the near energy-independence of the *NN* cross sections reduces the uncertainties in the extraction of radii. With FRIB400, the high sensitivity of the HRS for these experiments, and reaction theory developments, skin measurements on rare isotopes are expected to approach 0.05 fm accuracy.

3.2 Overcoming the threshold for pion production and new opportunities for Coulomb excitation

Some cross sections, such as the ones involving particle production, increase dramatically near threshold. Others increase more monotonously with energy and can become dominant at high energy: This is the case for Coulomb excitation cross sections populating giant resonances. The two sections below illustrate how FRIB400 will provide access to the low-energy dipole strength contained in the electric dipole (E1) resonance and present a new opportunity to possibly explore halos and skins in very neutron-rich nuclei using pion production.

3.2.1 Accessing low-energy dipole strength through Coulomb excitation

The isovector E1 giant dipole resonance (GDR) is perhaps the most studied of the giant resonances in nuclei [Har01]. Although the majority of the isovector E1 strength is contained in the main resonance, an enhancement of E1 strength observed at low excitation energies (see Figure 3.6), often referred to as the pygmy dipole resonance (PDR), has drawn most attention in recent years [Sav13] as it has implications for the study of neutron skins, the astrophysical *r* process, and the nuclear EOS [Bro00, Rei10, Pie13, Rei13].

FRIB400 will improve the study of nuclear resonances across the nuclear chart.

The combination of the high yields and high energies for very neutron-rich rare isotopes available at FRIB400 enables the excitation of such resonances, for example, with heavy-ion-induced Coulomb excitation at the HRS, in combination with the MoNA-LISA neutron detector array and γ-ray detection with arrays such as GRETA or CAESAR. At energies in excess of 300 MeV/u nucleon, the cross section for exciting the GDR via heavy-ion-induced Coulomb excitation increases rapidly and becomes dominant (see Figure 3.7).
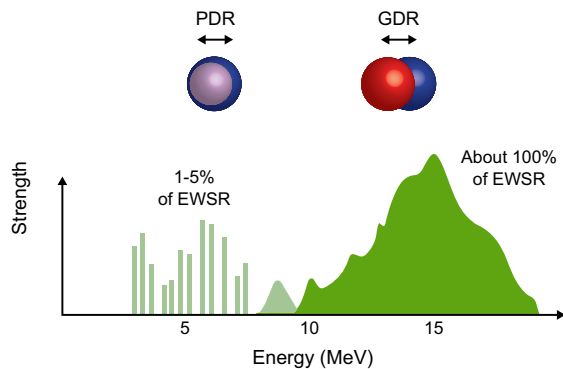
Figure 3.6: Schematics of the electric isovector dipole strength distribution in nuclei (Figure adapted with permission from Ref. [Zil15]). The majority of the strength (close to 100% of the energy-weighted sum rule) is associated with the giant dipole resonance (GDR), a minor fraction of the strength is attributed to the pygmy dipole resonance (PDR) near the particle-decay threshold.
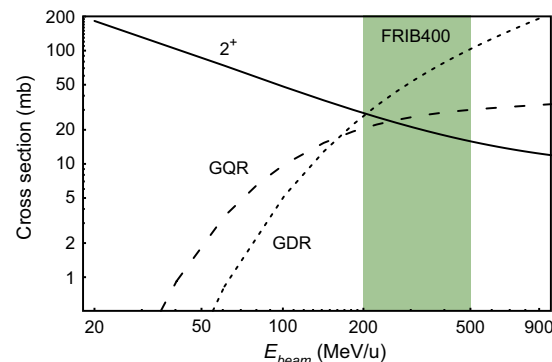
Figure 3.7: Heavy-ion Coulomb excitation cross sections for the first 2^+ state, the giant quadrupole resonance (GQR), and the GDR. FRIB400 makes it possible to perform experiments in the region where the excitation of the GDR becomes strong and dominant (figure adapted with permission from [Gla98]).

Coulomb-excitation studies at 0° in inelastic proton scattering will also become possible with FRIB400. Here, the response at forward center-of-mass scattering angles is investigated, allowing for an extraction of the full GDR response through missing-mass spectroscopy. Such data can be used to determine the dipole polarizability [Pie12, Rei10, Rei13] which is correlated with the neutron-skin thickness (see [Tam11] for an example). Measurements of the low-lying pygmy (PDR) dipole strength [Tam11, Pol12, Pie13, Rei13, Bir17] are critical

for the extraction of an accurate value of the dipole polarizability. Although the extraction of the neutron skin thickness through this method carries some model dependence, the ability to extend it to very neutron-rich systems makes it an attractive complement to other methods, including the electroweak measurements of neutron densities currently underway at Thomas Jefferson National Accelerator Laboratory [Hor14]. To extract the electric dipole strength from proton inelastic scattering experiments, it is important to minimize the impact of contributions from other excitations in the analysis. Beam energies around 300 MeV/u are optimal, because (i) the cross sections for Coulomb excitation of giant resonances are high and (ii) the contributions from excitations mediated by the nuclear force can be separated reliably [Pol12] in a multipole decomposition analysis, which benefits from the properties of the aforementioned *NN* interaction at these energies. FRIB400 will allow for such inelastic proton scattering experiments in inverse kinematics at 300 MeV/u, using the Active-Target Time Projection Chamber for detection of the low-energy recoil protons and the HRS for the detection of the fast projectile-like residues.

3.2.2 New degrees of freedom: Pion production as probe of skin and halo wave functions

The study of pion production in reactions on nuclei with thick skins or halos may provide unique insights into the details of the extended wave functions of such systems [Tar14]. This is based on the sensitivity of pion production cross sections and pion momentum distributions to the Fermi momentum of the nucleons. Pion production can be studied in reactions between a symmetric probe (e.g. ^{12}C) and a halo/skin nucleus [Li91]. At the energies available at FRIB400, such measurements will become possible.

Since, at energies below 1 GeV/u, pions are primarily produced through the Δ resonance [Ver79, Kit86], and since the inclusive production of charged pions depends predominantly on the *NN* interactions between nucleons in the probe and the impinging halo/skin system, the difference in π^- and π^+ production yields is sensitive to the proton and neutron density distributions of the skin/halo nucleus. Additional information can be obtained by comparing the momentum distributions of pions produced from isospin-symmetric nuclei to systems with thick skins or halos [Li91]. The sensitivity to the wave function of the skin/halo neutrons is strongest near the pion-production threshold and becomes small at beam energies around 600 MeV/u. Near-threshold energies of 200 to 400 MeV/u provide the right balance between production yields and sensitivity. FRIB400 would enable such experiments over the whole energy range for which the pion production yields and momentum distributions are most sensitive to halo or skin nucleons. Measurements could be performed with a time projection chamber placed in front of the HRS.

3.3 Kinematic focusing improves in-flight fission studies

Nuclear fission is an important, but complex, many-body process with significant impact on derivative nuclear technologies in the fields of nuclear energy, defense, and homeland security. Fission also shapes the elemental abundances in the Universe. The fission properties

of neutron-rich isotopes are important for the accurate modeling of nucleosynthesis in the r process, with impact on its end-point, on the abundance patterns in the region of fission fragments, and the final abundances of the heavy elements produced (see Section 1.4), including cosmochronometer isotopes, such as uranium and thorium [Thi83, Sch02]. Reliable data on the isotopic distribution of fission fragments is necessary to benchmark the fission models required to describe a variety of processes relevant for nuclear astrophysics, stockpile stewardship, and nuclear energy [Tal18, Sch16]. Kinematic focusing at FRIB400 will improve the simultaneous detection of both fragments in in-flight fission experiments at the HRS.

FRIB400 will allow a kinematically complete study of nuclear fission.

Recent theoretical work has investigated the sensitivity of fission model parameters to the prompt fission γ-ray spectrum (PFGS) [Tal12, Ste13a, Tal18] and is complemented by next-generation PFGS measurements in the major actinides [Jan13, Ull14, Obs13]. At FRIB, such experiments can be performed for neutron-rich heavy fissile systems by measuring in-flight produced fission fragments in the HRS in coincidence with prompt γ rays in GRETA, for example. Of particular interest is the ability to measure both fragments emitted in a fission event in coincidence, as it allows to test the detailed predictions of fission models, including correlations. The power of this method in benchmarking theoretical models was recently demonstrated with results from the SOFIA setup [Pel17] where both fission fragments were detected simultaneously.

Similar to the gains through kinematic focusing achieved in the production and transport of rare-isotope beams produced by in-flight fission (Section 5.4), the fission distribution and correlation studies strongly benefit from FRIB400, as the fission cone narrows and the ability to detect both in-flight fission fragments within the acceptance of the HRS increases. At 200 MeV/u, for example, it is possible to detect 77% of the fission pairs in the HRS, while at 400 MeV/u, the transmission will be 95%, achieving a near-complete characterization of the fission distribution for fissile neutron-rich nuclei. This will be particularly important for the study of weak branches and very asymmetric fission events.

4. Advantages of FRIB400 for isotope harvesting—impact on beyond-Standard-Model physics and applied programs

At the nominal isotope production energy of 200 MeV/u, FRIB will already provide a wide range of isotopes for research. This is due to the combination of a high-power heavy-ion linear accelerator coupled with in-flight production and separation, which offers advantages for efficient isotopic separation and a fast development time for the collection of any radionuclide. In addition, many important radionuclides will be produced in the water-filled beam dump and can be harvested for use in a variety of scientific fields, including nuclear astrophysics and the study of fundamental symmetries. Many of these radioisotopes also have applications that serve societal needs, in areas ranging from diagnosis and treatment of cancer to national security. The advantages of isotope collection and harvesting at FRIB are outlined in the whitepaper *"Isotope Harvesting at FRIB: Additional opportunities for scientific discovery"* [Abe18]. Appendix 1 of [Abe18]

Making isotopes available for electric dipole moment searches

FRIB will provide an unprecedented opportunity to search for permanent electric dipole moments (EDMs) of rare isotopes. FRIB400 will increase the yield for candidate nuclei, and so improve the statistical uncertainty on limits or perhaps even result in a measurement. It will also provide a greater opportunity to study systematic effects in challenging EDM searches.

EDMs violate both time-reversal (T) and parity (P) symmetries and, by the CPT theorem, charge conjugation-parity (CP) symmetry [Chu19]. CP-violation has long been thought to be one of the key ingredients needed to explain the matter-antimatter asymmetry of the visible Universe. Rare isotopes provide significant discovery potential for EDM searches because they amplify the observable EDM by orders of magnitude when compared to stable species. This implies that less stringent control of environment factors and systematic effects are required in order to enable a highly sensitive EDM search. Diamagnetic systems with octupole-deformed nuclei, such as Ra (radium), Rn (radon), and Pa (protactinium), are favorable candidates because the combination of their unusual nuclear structure and highly relativistic atomic structure amplifies the effects of CP-violating interactions originating within the nucleus by several orders of magnitude as compared to nearly spherical nuclei such as Hg or Xe [Aue96, Dob18].

FRIB will provide quantities of Ra and Rn that rival or are orders of magnitude larger than what is currently available. Some isotopes, such as Pa, will become available in sufficient quantities for the first time. In order to take full advantage of this upcoming opportunity, several technical, chemical, atomic, and nuclear-physics techniques will have to be developed in the intervening years. Because of the specific atomic structure of each of these isotopes and their different half-lives, a variety of different approaches will be required to collect the atoms, spin-polarize them, and then monitor the spin precession in order to perform the EDM searches. FRIB400 would directly result in over a factor of three increase in the number of atoms available, which is important for both developing new techniques, in particular for ^{229}Pa ($t_{1/2}$ = 1.5 days), and for studying systematic effects in ongoing EDM searches, in particular the ANL/MSU/USTC laser-trap based ^{225}Ra experiment [Bis16].

gives the full list of important isotopes. The advantages of FRIB and the importance of expanded research with rare isotopes was described in *"Meeting Isotope Needs and Capturing Opportunities for the Future"* [NSACi15].

FRIB400 will expand the scientific impact of harvested isotopes.

At FRIB400, all of the interesting isotopes listed in Appendix 1 of [Abe18] will increase by factors of 3 for separated isotopes and an order of magnitude for harvested isotopes. This significant increase would greatly improve statistics and accelerate the translational pace in biological studies that could be done, improve the sensitivity of measurements aimed at fundamental symmetry studies, or triple the number of rare-isotope devices that could be produced. In biology and medicine, FRIB400 could provide increased quantities of ^{52}Fe as a ^{52m}Mn generator. The ^{52}Fe/^{52m}Mn generator could make key contributions to many fields, including oncology, neurophysiology, and diabetes research owing to the critical role of manganese in biological systems [Her17, Nap17]. Given that this isotope is in short supply [NSACi15], additional gains of an order of magnitude with FRIB400 for harvested quantities are important. Other examples for gains are related to therapeutic successes with the α emitters ^{223}Ra and ^{225}Ac, highlighting the importance of additional access to α emitters such as ^{211}At with a gain of 4 to 10 with FRIB400, and Auger emitters like ^{119}Sb with a gain of a factor of 10.

One important fundamental area of isotope-enabled research is in the search for an intrinsic atomic electric dipole moment (EDM) (see the sidebar). EDMs are very sensitive observables that probe science beyond the Standard Model of Particle Physics, and could help to identify the reason for the matter-antimatter imbalance in the Universe. There are some specific candidate nuclei that would have enhanced sensitivity to these kinds of phenomena, and most of them are radioactive and hard to create, such as ^{225}Ra, ^{229}Pa, and ^{221,223}Rn.

For national security and other applications, the NSAC isotope report [NSACi15] states that *"[Isotopes] have become an indispensable part of the means we use to characterize nuclear processes, and are at the heart of probes used to interrogate suspect materials."* In this critical area, FRIB has advantages for isotopes like ^{48}V and ^{88}Zr [Shu19], where a detailed understanding of their nuclear reactions would enable a more detailed analysis of weapons-test results and more informative post-detonation nuclear forensics. The additional factor of 10 in harvested quantities of these isotopes would improve cross-section measurements by a factor of 3 and allow for weaker branches to be studied.

The increased availability of certain isotopes would enable further development and exploration of micro-electro-mechanical systems (MEMS). The ability to employ these transformational technology systems as portable, stand-alone devices in both normal and extreme environments depends upon the development of power sources compatible with the MEMS technology. This is where harvested isotopes play an important role in radioisotope micro power sources (RIMS). RIMS or "nuclear batteries" are top prospects for MEMS because they can operate for extended periods of time and in extreme environments. The upgrade would increase by factors of 3 to 10 the availability of candidate isotopes.

5. Technical overview of FRIB400

The FRIB energy upgrade to 400 MeV/u can be accomplished by adding additional cryomodules to the end of the FRIB linear accelerator (linac). This possibility was incorporated into the design of the linac tunnel during construction [CDR10]. As a result, the FRIB linac building includes 80 meters of space in the tunnel for additional cryomodules, which can accommodate the 11 cryomodules described below. If desired, the upgrade could be accomplished in stages by the addition of individual cryomodules as they become available. The additional cryomodules could be added in maintenance periods with no down-time for the facility and the science program.

FRIB400 design is technically ready and can be implemented without interruption of the science program.

The science requirements described in this document argue that the upgraded linac should be able to deliver a primary-beam energy of 400 MeV/u or higher for all ions in order reach the proper secondary-beam energies to enable the use of nuclear reactions at optimal energies. The higher energy also provides a significant increase in rare-isotope production. Over the past two years, a study of the possible technical solutions was performed to identify the best option for FRIB400 within the available real estate. Several types of superconducting (SC) cavities operating at different frequencies were investigated. It was concluded that a 5-cell 644-MHz cavity with $\beta_{opt} = 0.65$ is the optimal choice for FRIB400 for the following reasons [Ost18]:

- Allows for a low dynamic heat load with high accelerating voltage

- Lowest number of SC cavities to achieve 400 MeV/u for uranium

- Very efficient for acceleration of light ions and suitable for acceleration of protons up to nearly 1 GeV

- The cavity length is ~1m, which makes it suitable for cleaning and surface preparation with the existing infrastructure

- Most importantly, FRIB400 can be achieved within the available ~80-meter space by taking advantage of the proven performance of elliptical SC cavities

Because of the favorable features of the 644-MHz cavity, the development of such elliptical cavity at $\beta_{opt} = 0.65$ for FRIB400 has started. The parameters of the optimized cavity are listed in Table 5.1. Two SC cavities have been built in industry following our design and they are currently being processed and prepared for Dewar testing. A forthcoming conceptual design report will contain more details.

Table 5.1 Optimized cavity parameters for FRIB400.

Parameter	Value	Units
Frequency	644	MHz
Geometrical β	0.61	
Optimal β	0.65	
Aperture diameter	83	mm
Effective length (L_{eff})	71.0	cm
Number of cells	5	
Geometric shunt impedance R/Q	368	Ω
Geometry factor (G)	188	Ω
Peak surface electric field (E_{peak})	40	MV/m
Peak surface magnetic field (B_{peak})	77.5	mT
Accelerating gradient (E_{acc})	17.5	MV/m
Accelerating voltage at $β_{opt}$ (V_{acc})	12.4	MV
E_{peak}/E_{acc}	2.28	
B_{peak}/E_{acc}	4.42	mT/(MV/m)
Goal for the residual resistance	5	nΩ
BCS resistance at 2 K	2.7	nΩ
Dynamic heat load per cavity at 2 K	17.1	W
Number of cavities per cryomodule	5	
Number of cavities required	55	
Length of the focusing period (cryomodule plus warm section)	7.25	m
Total dynamic heat load at 2 K in upgrade segment of FRIB linac	938	W

5.1 Cavity design

Drawings of the jacketed cavity with slow and fast tuners are shown in Figure 5.1. The combined slow and fast tuner allows the resonant frequency of the cavity to be precisely tuned to the desired frequency by applying an axial force. The tuner design is based on work at Fermi National Accelerator Laboratory (FNAL) for slow and fast tuners developed for the 650-MHz PIP-II cavities [Pis18]. The tuner will be mounted on the helium vessel in the cryostat insulating vacuum space as shown in Figure 5.1. An electromechanical actuator drives the slow/coarse lever tuner; the actuator consists of a stepping motor, planetary gear box, and lead screw. Two piezo actuators are mounted on the tuner arm so that their force is applied directly to the cavity flange. A prototype tuner has been designed, fabricated, and tested at FNAL in collaboration with MSU [Con18]. The test results are consistent with the expectations based on the mechanical properties of the tuner.

A fundamental power coupler (FPC) was designed to deliver up to 15 kW of forward power to the cavity. The preliminary FPC design is shown in Figure 5.2. The beam loading in the

linac will require up to 4 kW of radio-frequency (RF) power per cavity. However, we have designed the FPC for up to 8 kW beam loading. This will allow for a possible future power upgrade of the FRIB linac to an 800 kW beam, split between two targets. An additional 7 kW of RF power will be available to compensate for possible microphonics detuning of the cavity. With this power and an external quality factor of 10^7, a 30-Hz bandwidth can be provided to mitigate microphonics. Extensive tests of the piezo-tuner are planned to determine whether a smaller bandwidth can be used which would allow for RF power below 15 kW.

The design of the FPC is based on the 20 kW RF coupler developed at Argonne National Laboratory (ANL) for 1.4-GHz elliptical cavities [Kel15]. This design is an evolution of well-established RF couplers with cold and warm windows which have been used successfully in TEM-class SRF cavities at lower power [Kel12]. The cold window provides cooling of the antenna by helium gas at ~50 K. The design of the FPC includes multi-physics optimization to provide sufficient cooling in the cold window such that temperature rises of the ceramic window and the antenna are reasonably low and minimize heat leaks into the 2 K liquid helium system. Currently, the detailed design of the FPC and modifications to the FRIB test cryostat for integrated testing of the jacketed elliptical cavity with the tuners and FPC are prepared.
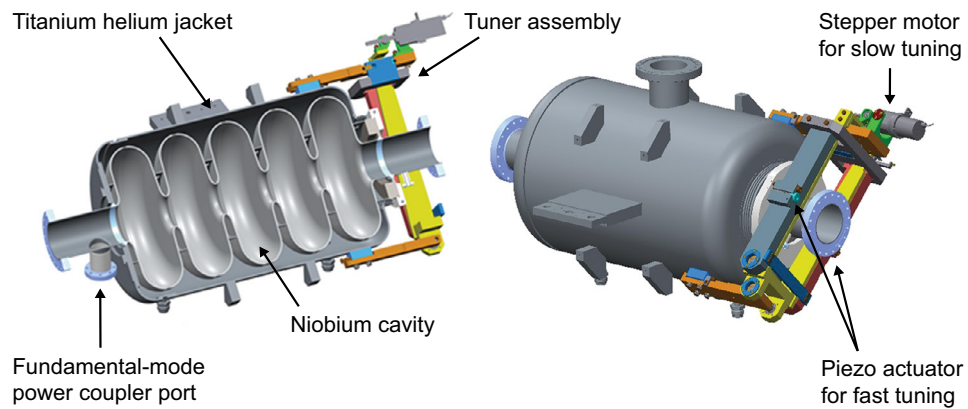

Figure 5.1: Proposed FRIB 644-MHz superconducting cavity in its helium vessel with slow and fast tuners.
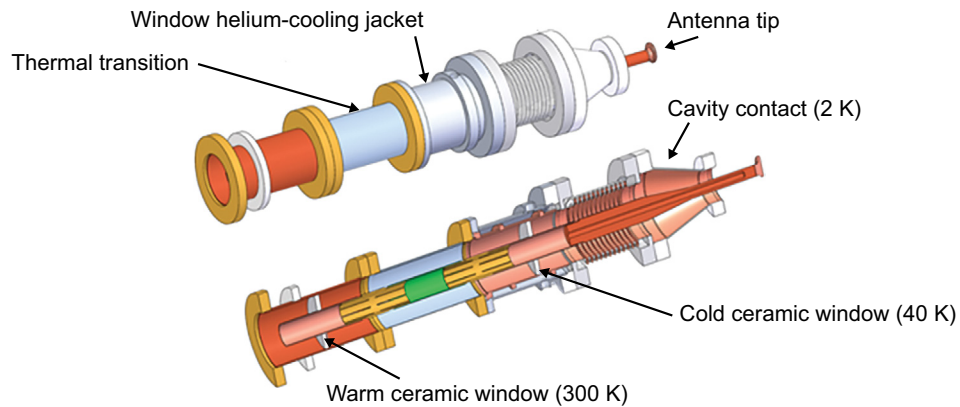
Figure 5.2: Main components of the 15 kW radio-frequency fundamental power coupler.

5.2 Beam dynamics

Due to the relatively high energy, the focusing period can be longer than for the FRIB half-wave resonator (HWR) cryomodules. Hence the upgrade cryomodule can house up to five cavities without cold focusing elements and the focusing can be provided by warm quadrupoles. As shown in Figure 5.3, each cryomodule is followed by a quadrupole doublet and a beam diagnostic box or steering magnet. In total, 11 cryomodules, 22 quadrupoles, 6 diagnostic boxes and 5 steering modules will be required over a total length of 79.2 m. Each quadrupole has an effective length of 0.25 m with a bore radius of 0.04 m, which results in pole-tip fields of less than 0.9 T. The linac layout in the tunnel with 11 upgrade cryomodules is shown in Figure 5.4.
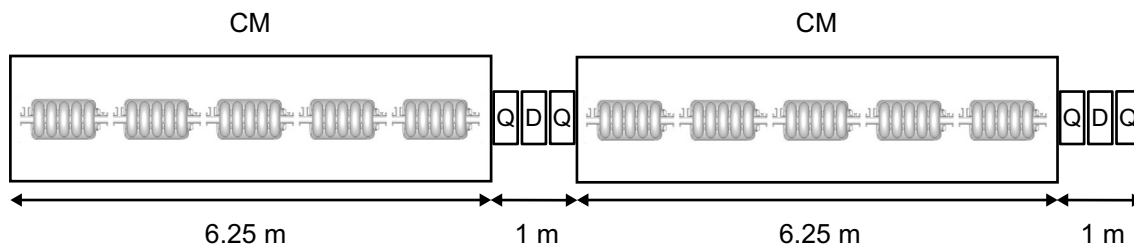
Figure 5.3: Proposed doublet lattice layout for FRIB400. The linac section will consist of a cryomodule (CM) with five cavities followed by quadrupoles (Q), and a diagnostics box (D) or steering module.
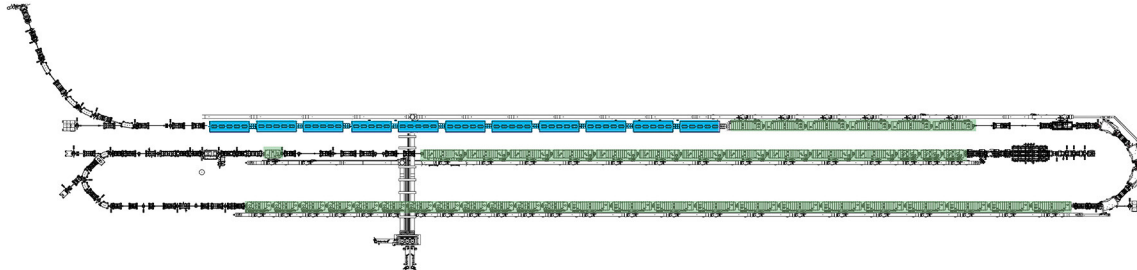
Figure 5.4: Footprint of the current (green and black) and upgraded (blue) FRIB linac.

Five charge states of uranium ($^{238}U^{76+}$ to $^{238}U^{80+}$) will be simultaneously accelerated along the upgrade section of the FRIB linac. A total of $2 \cdot 10^4$ particles of five-charge-state uranium were tracked in simulations from the first cryomodule of the upgrade section to the fragmentation target. The 3σ beam envelopes in both the horizontal and vertical planes are shown in Figure 5.5. The large physical aperture and large longitudinal acceptance of the cavities (see Figure 5.6) will minimize beam losses in the upgrade section. Beam energies of various ion species are listed in Table 5.2 at nominal FRIB beam energies and for FRIB400.
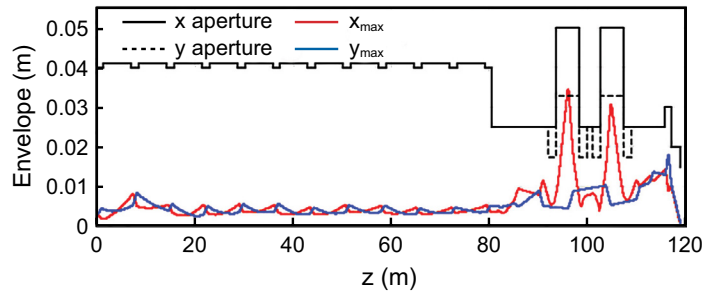
Figure 5.5: Drawn are 3σ beam envelopes of five different charge states of uranium in the upgraded section of the FRIB linac to the production target.
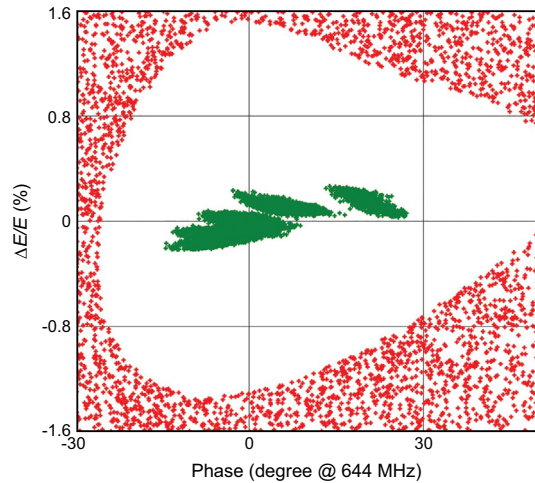
Figure 5.6: Longitudinal acceptance of the upgrade section of the linac (white area) with 5-charge-state uranium input beam (green).

Figure 5.7: Upgrade cavity installed on the tuning stand for bead pull measurements and field flatness tuning.

5.3 Cavity prototyping

Two SC cavities have been built in industry and were delivered to FRIB. Cavity #1 was electro-polished at the ANL chemistry facility and heat-treated at 600ºC in the MSU furnace. After heat treatment, the cavity was tuned for field flatness by plastically deforming individual cells using a dedicated fixture (Figure 5.7). Cavity #1 will be Dewar-tested in one of the FRIB test cryostats. The testing is expected to be completed in 2019. A similar process will be followed for Cavity #2 after buffered chemical polishing. In addition, it is planned to perform integrated testing of Cavity #2 with a helium vessel, slow and fast tuners, and FPC. Cavity #1 may undergo additional surface treatment and testing with the goal of developing a recipe to reduce the surface resistance for medium-frequency SC cavities.

5.4 Isotope production

The upgrade of the production energy to 400 MeV/u for uranium and higher for lighter ions will significantly enhance the production of rare isotopes. The gains have been investigated using the program LISE++ [Tar08]. The production energies assumed for each primary beam are listed in Table 5.2.

Table 5.2 Beam energies of various ion species (defined by atomic number *Z* and mass *A*) at FRIB and FRIB400.

Element	Z	A	FRIB	FRIB400	Element	Z	A	FRIB	FRIB400
O	8	16	320	587	Sn	50	124	235	463
O	8	18	281	533	Xe	54	124	252	490
Ne	10	20	320	587	Xe	54	136	221	440
Ne	10	22	287	542	Sm	62	144	242	474
Ar	18	36	320	587	Dy	66	156	234	462
Ar	18	40	285	539	Er	68	162	228	452
Ca	20	40	320	587	Yb	70	168	227	450
Ca	20	48	264	506	Yb	70	176	215	430
Ni	28	58	292	551	Os	76	184	220	438
Ni	28	64	268	512	Pt	78	190	220	438
Se	34	82	255	492	Pt	78	198	206	413
Kr	36	78	284	537	Hg	80	196	216	430
Kr	36	86	257	496	Hg	80	204	206	413
Zr	40	92	248	492	Pb	82	204	209	418
Mo	42	92	276	525	Pb	82	208	205	410
Cd	48	106	268	513	Bi	83	209	207	414
Sn	50	112	265	509	U	92	238	200	400

The gains in isotope production from increasing the FRIB beam energy from 200 to 400 MeV/u are illustrated in Figure 5.8. The gains are relative to the rates calculated for the FRIB facility before the energy upgrade [FRIBr]. The gains apply to fast-beam rates and may be applicable to reaccelerated-beam rates with an upgrade of the beam delivery system. The ratios shown in the figure were calculated using the optimum target for each fragment and 40 stable beams, indicated by black squares in the figure. Achieving the optimum target for all beams will require additional improvements in target technology. The gains are the result of the thicker production target over most of the chart. The yellow and black bands near atomic number 70 and 80 are the result of gains related to having more fully-stripped ions at higher energy. The gains in the region of fission fragments are due to the relatively smaller fission-fragment cone at higher energy through kinematic focusing. The gains at the extremes are the result of secondary production in the target. In this case, an initial fragment of the beam undergoes a secondary reaction to produce the fragment of interest. This effect can increase the production of very extreme isotopes by more than one order of magnitude, as shown in the figure.

The gains allow the dripline to be reached up to atomic number 60. Included in the new opportunities is the possibility to reach neutron-rich isotopes as exotic as ^{70}Ca (see Section 2.2). An additional advantage is that the higher energy allows for higher purity in the

separation of fragments. For example, isotopes such as ^{100}Sn, will be produced with a factor of 1,000 higher purity and will not require an RF separator as is the case at 200 MeV/u. The use of an RF separator reduces the available beam intensity. Specific examples of the new science made possible by the higher production yields and energy are given in the preceding science sections of this document.
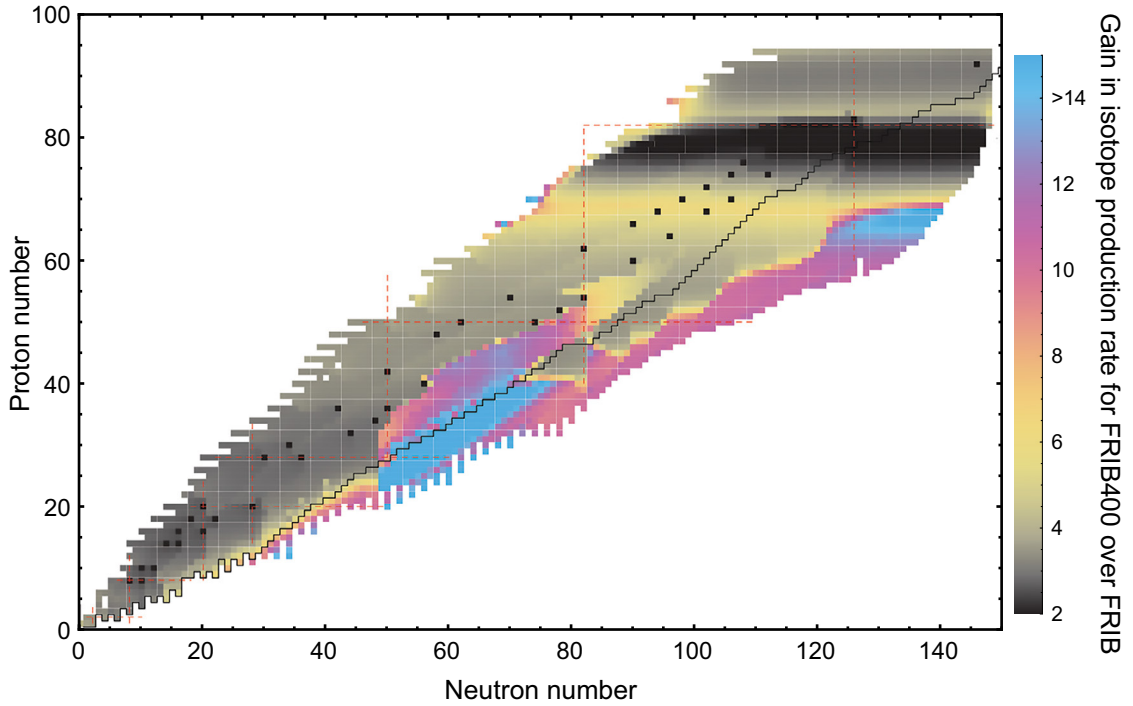

Figure 5.8: The gain in isotope production at FRIB400 relative to the nominal FRIB facility is shown. Gains are given for isotopes that are produced at rates of more than one atom per week.

References

[Abb17a]	B. P. Abbott *et al*., Astrophys. J. Lett. 848, L12 (2017)
[Abb17b]	B. P. Abbott *et al*., Phys. Rev. Lett. 119, 161101 (2017)
[Abb18]	B. P. Abbott *et al*., Phys. Rev. Lett. 121, 161101 (2018)
[Abe18]	E. P. Abel *et al*., arXiv:1812.03984; to be published in Journal of Physics G
[Afa13]	A. V. Afanasiev *et al*., Phys. Lett. B 726, 680 (2013)
[Ang13]	I. Angeli and K. P. Marinova, At. Data & Nucl. Data Tables 99, 69 (2013)
[Apr18]	A. Aprahamian *et al*., Proceedings for the FRIB Theory Alliance workshop "FRIB and the GW170817 kilonova", held 16-27 July 2018 at the Facility for Rare Isotope Beams, Michigan State University, East Lansing, MI USA; arXiv:1809.00703
[Arc17]	I. Arcavi *et al*., Nature 551, 64 (2017)
[Ata18]	L. Atar *et al*., Phys. Rev. Lett. 120, 052501 (2018)
[Aue96]	N. Auerbach *et al*., Phys. Rev. Lett. 76, 4316 (1996)
[Aum13]	T. Aumann *et al*, Phys. Rev. C 88, 064610 (2013)
[Bar17]	I. Bartos and M. Kowalski, Multimessenger Astronomy, IOP Publishing (2017) http://dx.doi.org/10.1088/978-0-7503-1369-8
[Bau17]	A. Bauswein *et al*., Astrophys. J. Lett. 850, L34 (2017)
[Bio87]	R. M. Bionta *et al*., Phys. Rev. Lett. 58, 1494 (1987)
[Bir17]	J. Birkhan *et al*., Phys. Rev. Lett. 118, 252501 (2017)
[Bis16]	M. Bishof *et al*., Phys. Rev. C 94, 025501 (2016)
[Bla05]	D. Blaschke *et al*., Phys. Dev. D. 72, 065020 (2005)
[Bol17]	R. Bollig *et al*., Phys. Rev. Lett. 119, 242702 (2017)
[Bov17]	L. Bovard *et al*., Phys. Rev. D 96, 124005 (2017)
[Bro98]	B. A. Brown, Phys. Rev. C 58, 220 (1998)
[Bro09]	E. F. Brown and A. Cumming, Astrophys. J. 698, 1020 (2009)
[Bro00]	B. A. Brown, Phys. Rev. Lett. 85, 5296 (2000)
[Bro10]	B. A. Brown, Physics Viewpoint: Islands of insight in the nuclear chart, Physics 3, 104 (2010)
[Bro17]	B. A. Brown, Phys. Rev. Lett. 119, 122502 (2017)
[Cac06]	E. M. Cackett *et al*., MNRAS 372, 479 (2006)
[Car19]	Z. Carson *et al*., Phys. Rev. D 99, 043010 (2019)
[CDR10]	Conceptual Design Report, FRIB-Z00000-AD-000049-R003, Issued 11 Aug 2010
[Cha01]	http://chandra.harvard.edu/photo/2001/ks1731 (retrieved June 2019)
[Cha08]	N. Chamel *et al*., Living Rev. Relativ. 11, 10 (2008)
[Che14]	W. Chen and J. Piekarewicz, Phys. Rev. C 90, 044305 (2014)
[Chu19]	T. E. Chupp *et al*., Rev. Mod. Phys. 91, 015001 (2019) and references therein
[Cir18]	V. Cirigliano *et al*., Phys. Rev. Lett. 120, 202001 (2018)

[Con18]   C. Contreras, "Testing of slow/fast tuner for medium beta elliptical cavities", FNAL internal report, November 2018

[Cot18]   B. Côté *et al.*, Astrophys. J. 855, 99 (2018)

[Cow98]   A. A. Cowley *et al.*, Phys. Rev. C 57, 3185 (1998)

[Cow19]   J. J. Cowan *et al.*, submitted to Rev. Mod. Phys. (2019); arXiv:1901.01410

[Coz18]   D. M. Cozma, Eur. Phys. J. A 54, 40 (2018)

[Cyb16]   R. H. Cyburt *et al.*, Astrophys. J. 830, 55 (2016)

[Dan00]   P. Danielewicz, Nucl. Phys. A, 673, 375 (2000)

[Dan02]   P. Danielewicz *et al.*, Science 298, 1592 (2002)

[De18]   S. De *et al.*, Phys. Rev. Lett. 121, 091102 (2018)

[Deg14]   N. Degenaar *et al.*, Astrophys. J. 791, 47 (2014)

[Dem10]   P. B. Demorest *et al.*, Nature 467, 1081 (2010)

[Den18]   P. Denissenkov *et al.*, J. Phys. G 45, 055203 (2018)

[Dei17]   A. Deibel *et al.*, Astrophys. J. 839, 95 (2017)

[Dia18]   P. Díaz Fernández *et al.*, Phys. Rev. C 97, 024311 (2018)

[Dob07]   J. Dobaczewski *et al.*, Prog. Part. Nucl. Phys. 59, 432 (2007)

[Dob18]   J. Dobaczewski *et al.*, Phys. Rev. Lett. 121, 232501 (2018)

[Due18]   M. Duer for the CLAS collaboration, Nature 560, 617 (2018)

[Eng17]   J. Engel and J. Menéndez, Rep. Prog. Phys. 80, 046301 (2017)

[Erl12]   J. Erler *et al.*, Nature 486, 509 (2012)

[Erl13]   J. Erler *et al.*, Phys. Rev. C 87, 044320 (2013)

[Est14]   A. Estradé *et al.*, Phys. Rev. Lett. 113, 132501 (2014)

[Fat18]   F. J. Fattoyev *et al.*, Phys. Rev. Lett. 120, 172702 (2018)

[FDS]   The FRIB Decay Station White paper; https://indico.frib.msu.edu/event/2/attachments/43/209/FRIB_Decay_Station_WP.pdf

[FME]   FRIB Mass explorer, http://massexplorer.frib.msu.edu/

[For13]   C. Forssén *et al.*, Phys. Scr. T152, 014022 (2013)

[Fra85]   M. A. Franey and W. G. Love, Phys. Rev. C 31, 488 (1985)

[Fuc06]   C. Fuchs, Prog. Part. Nucl. Phys. 56, 1 (2006)

[FRIBr]   FRIB Rates online at https://groups.nscl.msu.edu/frib/rates/fribrates106.html

[Fuj18]   S. Fujibayashi *et al.*, Astrophys. J. 860, 64 (2018)

[Fur02]   R. J. Furnstahl, Nucl. Phys. A 706, 85 (2002)

[Gaa81]   C. Gaarde *et al.*, Nucl. Phys. A 369, 258 (1981)

[Gaa85]   C. Gaarde, Proc. Niels Bohr Centennial Conference on Nuclear Structure, Copenhagen, 449c (1985)

[Gan12]   S. Gandolfi *et al.*, Phys. Rev. C 85, 032801(R) (2012)

[Gan15]   S. Gandolfi *et al.*, Annu. Rev. Nucl. Part. Phys. 65, 303 (2015)

[Gla98]   T. Glasmacher, Annu. Rev. Nuc. Part. Sci. 48, 1 (1998)

[Gor13]   S. Goriely *et al.*, Phys. Rev. C 88, 024308 (2013)

[Gre]   Gamma-Ray Energy Tracking Array, http://greta.lbl.gov/

[Gys19]   P. Gysbers *et al.*, Nat. Phys. 15, 428 (2019)

[Hag13]   G. Hagen *et al.*, Phys. Rev. Lett. 111, 132501 (2013)

[Hag14]   G. Hagen *et al.*, Phys. Rev. C 89, 014319 (2014)

[Hal17]   G. Hallinan *et al.*, Science 358, 1579 (2017)

[Han17]   M. Hanauske *et al.*, Phys. Rev. D 96, 043004 (2017)

[Han87]   P. G. Hansen and B. Jonson, Euro. Phys. Lett. 4, 409 (1987)

[Har01]   M. N. Harakeh and A. van der Woude, Giant Resonances, Fundamental High-Frequency Modes of Nuclear Excitations, Oxford Studies in Nuclear Physics 24, Clarendon Press, Oxford, 2001

[Hat97]   K. Hatanaka *et al.*, Phys. Rev. Lett. 78, 1014 (1997)

[Heb13]   K. Hebeler *et al.*, Astrophys. J. 773, 11 (2013)

[Hen17]   O. Hen *et al.*, Rev. Mod. Phys. 89, 045002 (2017)

[Her17]   R. Hernandez *et al.*, Diabetes 66, 2163 (2017)

[Hey11]   K. Heyde and J. L. Wood, Rev. Mod. Phys. 83, 1467 (2011)

[Hir87]   K. Hirata *et al.*, Phys. Rev. Lett. 58, 1490 (1987)

[Hol19]   J.D. Holt *et al.*, submitted (2019); arXiv:1905.10475

[Hon14]   Jun Hong and P. Danielewicz, Phys. Rev. C 90, 024605 (2014)

[Hor14]   C. J. Horowitz *et al.*, Eur. Phys. J A 50, 48 (2014)

[Hor15]   C. J. Horowitz *et al.*, Phys. Rev. Lett. 114, 031102 (2015)

[Hor19]   C. J. Horowitz *et al.*, J. Phys. G, in press (2019); arXiv:1805.04637

[HRS]   High Rigidity Spectrometer for FRIB, http://hrs.lbl.gov/

[Jan13]   M. Jandel *et al.*, Los Alamos Report LA-UR-12-24975, 2013

[Jus15]   O. Just *et al.*, MNRAS 448, 541 (2015)

[Jos10]   J. Jose *et al.*, Astrophys. J. Suppl. 189, 204 (2010)

[Kas17]   D. Kasen *et al.*, Nature 551, 80 (2017)

[Kel12]   M. P. Kelly *et al.*, Proc. of LINAC'12, p. 678

[Kel15]   M. P. Kelly *et al.*, Proc. of SRF'15, p. 1346

[Kit86]   Y. Kitazoe *et al.*, Phys. Lett. B 166, 35 (1986)

[Kor13]   M. Kortelainen *et al.*, Phys. Rev. C 88, 031305(R) (2013)

[Kre95]   G. Krein *et al.*, Phys. Rev. C 51, 2646 (1995)

[Lan03]   K. Langanke and G. Martinez-Pinedo, Rev. Mod. Phys. 75 819 (2003)

[Lat01]   J. M. Lattimer and M. Prakash, Astrophys. J. 550, 426 (2001)

[Lat04]   J. M. Lattimer and M. Prakash, Science 304, 536 (2004)

[Lau18]   R. Lau *et al.*, Astrophys. J. 859, 62 (2018)

[Len10]   S. M. Lenzi *et al.*, Phys. Rev. C 82, 054301 (2010)

[Lef16]   A. Le Fèvre *et al.*, Nucl. Phys. A 945, 112 (2016)

[Li91]	B-A. Li *et al*., Nucl. Phys. A 533, 749 (1991)
[Li00]	B-A. Li, Phys. Rev. Lett. 85, 4221 (2000)
[Li14]	Topical issue on nuclear symmetry energy, Eds. Bao-An Li *et al*., Eur. Phys. J. A 50, 9 (2014)
[Lid16]	S. N. Liddick *et al*., Phys. Rev. Lett. 116, 242502 (2016)
[Lip18]	S. Lipschutz, to be published, and PhD thesis, MSU, 2018
[LRP15]	DOE/NSF NSAC Long Range Plan, Reaching for the Horizon: The 2015 Long Range Plan for Nuclear Science, October 2015
[Lyn09]	W. G. Lynch *et al*., Prog. Part. Nucl. Phys. 62, 427 (2009)
[Lyn18]	W. G. Lynch, M. B. Tsang, submitted (2018); arXiv:1805.10757
[Mar15]	D. Martin *et al*., Astrophys. J. 813, 2 (2015)
[Mar16]	J. Marganiec *et al*., Phys. Rev. C 93, 045811 (2016)
[Mei18]	Z. Meisel *et al*., J. Phys. G Nucl. Phys. 45, 093001 (2018)
[Mey81]	J. Meyer-Ter-Vehn, Phys. Rep. 74, 323 (1981)
[Mig78]	A. B. Migdal, Rev. Mod. Phys. 50, 107 (1978)
[Mil19]	A. J. Miller *et al*., Nature Phys. (2019)
[Mir16]	A. Mirizzi *et al*., Rivista del Nuovo Cimento 39, 1 (2016)
[Mum16]	M. R. Mumpower *et al*., Prog. Part. Nucl. Phys. 86, 86 (2016)
[Mus16]	M. T. Mustonen and J. Engel, Phys. Rev. C 93, 014304 (2016)
[NaD13]	Committee on the Assessment and Outlook for Nuclear Physics, Nuclear Physics: Exploring the Heart of Matter, Decadal Study, The National Academies Press (2013)
[Nap17]	H. Napieczynska *et al*., Neuroimage 158, 112 (2017)
[Naz16]	W. Nazarewicz, J. Phys. G 43, 044002 (2016)
[Neu18]	L. Neufcourt *et al*., Phys. Rev. C 98, 034318 (2018)
[Neu19]	L. Neufcourt *et al*., Phys. Rev. Lett. 122, 062502 (2019)
[Now16]	F. Nowacki *et al*., Phys. Rev. Lett. 117, 272501 (2016)
[NRC07]	Rare-Isotope Science Assessment Committee, Scientific Opportunities with a Rare-Isotope Facility in the United States, Board on Physics and Astronomy, National Research Council of The National Academies (The National Academies Press: Washington, D.C., 2007)
[NSACi15]	NSAC-Isotopes Subcommittee, Meeting isotope needs and capturing opportunities for the future: The 2015 Long Range Plan for the DOE-NP Isotope program (DOE 2015)
[NSAC07]	NSAC Subcommittee, Report to NSAC of the Rare-Isotope Beam Task Force (2007)
[Obe14]	A. Obertelli *et al*., Eur. Phys. J A 50, 8 (2014)
[Oer17]	M. Oertel *et al*., Rev. Mod. Phys. 89, 015007 (2017)
[Ost18]	P. N. Ostroumov *et al*., Nucl. Instrum. Meth. Phys. Res., A 888, 53 (2018)
[Ost92]	F. Osterfeld, Rev. Mod. Phys. 64, 491 (1992)

[Oza01]   A. Ozawa *et al*., Nucl. Phys. A 693, 32 (2001)

[Pan16]   V. Panin *et al*., Phys. Lett. B 753, 204 (2016)

[Pel17]   E. Pellereau *et al*., Phys. Rev. C 95, 054603 (2017)

[Pet95]   C. J. Pethick *et al*., Nucl. Phys. A 584, 675 (1995)

[Pia17]   E. Pian *et al*., Nature 551, 67 (2017)

[Pie13]   J. Piekarewicz, J. Phys.: Conf. Ser. 420, 012143 (2013)

[Pis18]   Y. M. Pischalnikov *et al*., Proc. of IPAC'18, p. 2671

[Pie19]   J. Piekarewicz and F. J. Fattoyev, Phys. Rev. C 99, 045802 (2019)

[Pol12]   I. Poltoratska *et al*., Phys. Rev. C 85, 041304(R) (2012)

[Pra88]   M. Prakash *et al*., Phys. Rev. Lett. 61, 2518 (1988)

[Rad16]   D. Radice *et al*., MNRAS 460, 3255 (2016)

[Rad18]   D. Radice *et al*., Astrophys. J. Lett. 852, L29 (2018)

[Rap06]   W. Rapp *et al*., Rep. Prog. Phys. Astrophys. J. 653, 474 (2006)

[Rav83]   D. G. Ravenhall *et al*., Phys. Rev. Lett. 50, 2066 (1983)

[Rei07]   W. Reisdorf *et al*., Nucl. Phys. A 781, 459 (2007)

[Rei10]   P.-G. Reinhard and W. Nazarewicz, Phys. Rev. C 81, 051303(R) (2010)

[Rei13]   P.-G. Reinhard and W. Nazarewicz, Phys. Rev. C 87, 014324 (2013)

[Rob12]   L. F. Roberts *et al*., Phys. Rev. Lett. 108, 061103 (2012)

[Ros99]   S. Rosswog *et al*., Astron. Astrophys. 341, 499 (1999)

[Rui16]   R. F. Garcia Ruiz *et al*., Nature Phys. 12, 594 (2016)

[Rus16]   P. Russotto *et al*., Phys. Rev. C 94, 034608 (2016)

[Sas11]   M. Sasano *et al*., Phys. Rev. Lett. 107, 202501 (2011)

[Sas12]   M. Sasano *et al*., Phys. Rev. C 86, 034324, (2012)

[Sav13]   D. Savran *et al*., Prog. Part. Nucl. Phys. 70, 210 (2013)

[Sch98]   H. Schatz *et al*., Phys. Rep. 294, 167 (1998)

[Sch02]   H. Schatz *et al*., Astrophys. J. 579, 626 (2002)

[Sch13]   H. Schatz *et al*., Nature 505, 62 (2013)

[Sch16]   N. Schunck and L. M. Robledo, Rep. Prog. Phys. 79, 116301 (2016)

[Sht07]   P. S. Shternin *et al*., MNRAS 382, L43 (2007)

[Shu19]   J. A. Shustermann *et al*., Nature 565, 328 (2019)

[Sie17]   D. M. Siegel and B. D. Metzger, Phys. Rev. Lett. 119, 231102 (2017)

[Sma17]   S. J. Smartt *et al*., Nature 551, 75 (2017)

[SP14]   U.S. Department of Energy Strategic Plan (2014 – 2018), https://www.energy.gov/
            downloads/2014-2018-strategic-plan (retrieved June 2019)

[Spy14]   A. Spyrou *et al*., Phys. Rev. Lett. 113, 232502 (2014)

[Ste13]   I. Stetcu *et al*., Phys. Rev. C 88, 044603 (2013)

[Suh17]   J. T. Suhonen, Front. Phys. 5, 55 (2017) and references therein.

[Sur06]   R. Surman *et al*., Astrophys. J., 643, 1057 (2006)

[Sur14]   R. Surman *et al*., AIP Advances 4, 041008 (2014)

[Sur18]   R. Surman and M. R. Mumpower, EPJ Web of Conferences 178, 04002 (2018)

[Tad87]   T. N. Taddeucci *et al*., Nucl. Phys. A469, 125 (1987)

[Tal12]   P. Talou *et al*., Proceedings of the 5th International Conference on Fission, Sanibel Island, Nov. 2012, pp. 581

[Tal18]   P. Talou *et al*., Eur. Phys. J. A 54, 9 (2018)

[Tam11]   A. Tamii *et al*., Phys. Rev. Lett. 107, 062502 (2011)

[Tan85]   I. Tanihata *et al*., Phys. Rev. Lett. 55, 2676 (1985)

[Tan18]   M. Tanabashi *et al*. (Particle Data Group), Phys. Rev. D 98, 030001 (2018)

[Tan19]   R. Taniuchi *et al*., Nature 569, 53 (2019)

[Tar08]   O. B. Tarasov and D. Bazin, Nucl. Instrum. Meth. Phys. Res. B 266, 4657 (2008) and http://lise.nscl.msu.edu/lise.html

[Tar14]   C. M. Tarbert *et al*., Phys. Rev. Lett. 112, 242502 (2014)

[Tar18]   O. B. Tarasov *et al*., Phys. Rev. Lett. 121, 022501 (2018)

[Tew17]   I. Tews *et al*., Astrophys. J. 848, 105 (2017)

[Thi83]   F.-K. Thielemann *et al*., Z. Phys. A 309, 301 (1983)

[Thi17]   F.-K. Thielemann *et al*., Ann. Rev. Nucl. Part. Sci. 67, 253 (2017)

[Tro17]   E. Troja *et al*., Nature 551, 71 (2017)

[Tsa17]   M. B. Tsang *et al*., Phys. Rev. C 95, 044614 (2017)

[Tsa19a]   C. Y. Tsang *et al*., Phys. Lett. B, in press (2019); arXiv:1901.07673

[Tsa19b]   M. B. Tsang *et al*., Phys. Lett. B, in press (2019); arXiv:1906.02180

[Tur15]   A. Turlione *et al*., Astron. Astrophys. 577, A5 (2015)

[Ube14]   E. Uberseder *et al*., Phys. Rev. Lett. 112, 211101 (2014)

[Ull14]   J. L. Ullmann *et al*., Phys. Rev. C 89, 034603 (2014)

[Ver80]   B. J. VerWest and R. A. Arndt, Phys. Rev C 25, 1979 (1980)

[Wal81]   R. K. Wallace and S. E. Woosley, Astrophys. J. Suppl. 45, 389 (1981)

[Wan14]   Shinya Wanajo *et al*., Astrophys. J. 789, L39 (2014)

[Wan17]   Meng Wang *et al*., Chin. Phys. C 41, 030003 (2017)

[Wes16]   S. Wesolowski *et al*., J. Phys. G 43, 074001 (2016)

[Woo04]   S. E. Woosley *et al*., Astrophys. J. Suppl. 151, 75 (2004)

[Xu16]   J. Xu *et al*., Phys. Rev. C 93, 044609 (2016)

[Yam11]   T. Yamaguchi *et al*., Phys. Rev. Lett. 107, 032502 (2011)

[Yas18]   J. Yasuda *et al*., Phys. Rev. Lett. 121, 132501 (2018)

[Zha14]   Y. Zhang *et al*., Phys. Lett. B 732, 186 (2014)

[Zha18]   T. Zhao and J.M. Lattimer, Phys. Rev. D 98, 063020 (2018)

[Zil15]   A. Zilges, J. Phys.: Conf. Ser. 590, 012006 (2015)

Appendix 1: The "Science with a 400 MeV/u upgrade of FRIB" workshop and whitepaper

The workshop *"Science with a 400 MeV/u upgrade of FRIB"* was held on August 9, 2018 in conjunction with the 2018 Low Energy Community Meeting in East Lansing, Michigan. The workshop initiated the science discussions and subsequent emails solicited input for this whitepaper from the registrants of the workshop, the FRIB Users Organization, and the FRIB Theory Alliance.

Workshop organizers: A. Gade and B. M. Sherrill (NSCL)

Agenda	Speaker
Introduction: 400 MeV/u upgrade for FRIB	Brad Sherrill (NSCL)
Advantages for *r*-process studies	Matt Mumpower (LANL)
Advantages for equation-of-state studies	Bao-An Li (TAMU-Commerce)
Advantages for reactions and reaction mechanisms	Remco Zegers (NSCL)
Discussion	

Unanimously adopted resolution:

We strongly support pursuit of the 400 MeV/u energy upgrade of FRIB. It will open new scientific opportunities and is timely given the recent neutron-star merger observation.

The "Science with a 400 MeV/u upgrade of FRIB" workshop registrants and attendees, and contributors to this whitepaper

Name	Affiliation
DeukSoon Ahn	RIKEN, Japan
Sunghoon (Tony) Ahn	Cyclotron Institute, Texas A&M University
Tan Ahn	University of Notre Dame
Jacob Allen	University of Notre Dame
Matt Amthor	Bucknell University
John Ash	FRIB, Michigan State University
Jonathan Barney	FRIB, Michigan State University
Thomas Baumann	FRIB, Michigan State University
Georg Berg	University of Notre Dame
Jill Berryman	FRIB, Michigan State University
Scott Bogner	FRIB, Michigan State University
Georg Bollen	FRIB, Michigan State University
Maxime Brodeur	University of Notre Dame
B. Alex Brown	FRIB, Michigan State University
Christopher Campbell	Lawrence Berkeley National Laboratory
Michael Carpenter	Argonne National Laboratory
Richard Casten	Yale University and FRIB, Michigan State University
Zbigniew Chajecki	Western Michigan University
Bob Charity	Washington University in St. Louis
Heather Crawford	Lawrence Berkeley National Laboratory
Mario Cromaz	Lawrence Berkeley National Laboratory
Pawel Danielewicz	FRIB, Michigan State University
Catherine Deibel	Louisiana State University
Paul DeYoung	Hope College
Iris Dillmann	TRIUMF, Canada
Charlotte Elster	Ohio University
Jutta Escher	Lawrence Livermore National Laboratory
Mike Famiano	Western Michigan University
Michael Febbraro	Oak Ridge National Laboratory
Charles Folden	Cyclotron Institute, Texas A&M University
Bogdan Fornal	INP, Polish Academy of Sciences, Krakow, Poland
Nathan Frank	Augustana College
Alexandra Gade	FRIB, Michigan State University
Bingshui Gao	FRIB, Michigan State University
Tom Ginter	FRIB, Michigan State University
Thomas Glasmacher	FRIB, Michigan State University

John Greene	Argonne National Laboratory
Paul Gueye	FRIB, Michigan State University
Kerim Gulyuz	Central Michigan University
Wolfgang Hennig	XIA LLC
Matthew Hill	FRIB, Michigan State University
Hironori Iwasaki	FRIB, Michigan State University
Robert V. F. Janssens	University of North Carolina – Chapel Hill
Genie Jhang	FRIB, Michigan State University
Ritu Kanungo	Saint Mary's University in Halifax
Filip Kondev	Argonne National Laboratory
Elaine Kwan	FRIB, Michigan State University
Kyle Leach	Colorado School of Mines
Hye Young Lee	Los Alamos National Laboratory
Silvia Leoni	INFN Milano, Italy
Shelly Lesher	University of Wisconsin La Crosse
Bao-An Li	Texas A&M University - Commerce
Brenden Longfellow	FRIB, Michigan State University
Walter Loveland	Oregon State University
Rebeka Sultana Lubna	Florida State University
William G. Lynch	FRIB, Michigan State University
Paul Mantica	FRIB, Michigan State University
Scott Marley	Louisiana State University
Zach Meisel	Ohio University
David J. Morrissey	FRIB, Michigan State University
Matt Mumpower	Los Alamos National Laboratory
Witold Nazarewicz	FRIB, Michigan State University
Shumpei Noji	FRIB, Michigan State University
Filomena Nunes	FRIB, Michigan State University
Wei Jia Ong	Argonne National Laboratory
Peter Ostroumov	FRIB, Michigan State University
Steve Pain	Oak Ridge National Laboratory
Jorge Pereira	FRIB, Michigan State University
Maria Piarulli	Argonne National Laboratory
Jorge Piekarewicz	Florida State University
Matthew Redshaw	Central Michigan University
Andrea Richard	FRIB, Michigan State University
Luke Roberts	FRIB, Michigan State University
Clementine Santamaria	FRIB, Michigan State University
Guy Savard	Argonne National Laboratory
Hendrik Schatz	FRIB, Michigan State University

Greg Severin   FRIB, Michigan State University
Bradley Sherrill   FRIB, Michigan State University
Jaideep Singh   FRIB, Michigan State University
Mallory Smith   FRIB, Michigan State University
Artemis Spyrou   FRIB, Michigan State University
Rebecca Surman   University of Notre Dame
Sean Sweany   FRIB, Michigan State University
Oleg Tarasov   FRIB, Michigan State University
Betty Tsang   FRIB, Michigan State University
Chun Yuen (Tommy) Tsang   FRIB, Michigan State University
Robert Varner   Oak Ridge National Laboratory
Jie Wei   FRIB, Michigan State University
Dirk Weisshaar   FRIB, Michigan State University
Michael Wiescher   University of Notre Dame
Robert Wiringa   Argonne National Laboratory
Chris Wrede   FRIB, Michigan State University
Hongyi Wu   Peking University, China
Jin Wu   Argonne National Laboratory
Isaac Yandow   FRIB, Michigan State University
Sherry Yennello   Cyclotron Institute, Texas A&M University
Remco Zegers   FRIB, Michigan State University
Vladimir Zelevinsky   FRIB, Michigan State University

Appendix 2: The "Nuclear Equation of State" workshop

A workshop on the status and future of equation-of-state studies was held on June 28, 2018 in Detroit. The workshop assessed the status, efforts, and opportunities within this subfield of rare-isotope science with the aim to determine what can be learned from experiment, theory, and astrophysical observations in the next decade and to evaluate what resources will become available and what additional resources will be needed. Results from this meeting were input to the corresponding presentation at the *"Science with a 400 MeV/u upgrade of FRIB"* workshop and are included in the section of this whitepaper.

Workshop organizers: W.G. Lynch and M.B. Tsang (NSCL)

	Agenda	Speaker
	Welcome	Lynch
Neutron star mergers:	Chatziioannou, Radice, Reddy, Tews, Horowitz, Piekarewicz	
	What is the current status of the constraints on the EOS?	Horowitz
	What property of the EOS does the merger signal probe now and in the future?	Radice
	What new developments and new capabilities can we expect to see in the next decade?	Chatziioannou, Radice
	What instruments present and new are needed for these observations?	Chatziioannou, Radice
	Discussion	Garg
	Coffee Break	
Neutron star and supernova observations:	Chatziioannou, Radice, Horowitz, Roberts, Brown, Prakash	
	How has the field progressed from Steiner *et al.*?	Brown
	What densities and what EOS properties determine each observable?	Horowitz
	What relevant new astronomical information can we hope to obtain in the next decade?	Brown
	What is the status and what are the prospects for neutrino-sphere EOS	Roberts
	What instruments are needed for these observations?	Brown
	Discussion	Radice
Experiment probes:	Tsang, Lynch, Natowitz, Yennello, Chajecki, Garg	
	Status of current experimental results on EOS	Tsang
	Status of facilities/instruments/observables	Lynch

	Skins, GDR, fission	Piekarewicz, Garg, Danielewicz, Chajecki
	What new observables and new experimental opportunities and results can be expected in the next decade?	Chajecki
	What facilities and instruments are needed for these measurements	Chajecki, Garg, Yennello
	What densities and what aspect of the EOS do these observables probe?	Lynch, Danielewicz
	Discussion	Natowitz
	Lunch	
Theory:	Danielewicz, Li, Ko, Tews, Reddy, Holt, Prakash, Piekarewicz	
	What are the theoretical questions regarding the EOS that should be addressed in the next decade?	Li
	Temperature dependence of EOS? High temperature proto-neutron star?	Prakash, Li
	What theoretical developments of EOS are needed and at which density regions (crust, core, etc.)?	Horowitz, Piekarewicz
	What theoretical developments are needed to address questions regarding neutron stars and mergers?	Tews, Piekarewicz
	What theoretical developments are needed to address questions regarding core-collapse supernovae?	Roberts
	Status of transport models	Ko
	Experimental observables: pion ratios; n, p differential flows; kaons, particle correlations	Danielewicz
	Discussion	Roberts
Interdisciplinary:	Role of JINA, INT, FRIB Theory Alliance in these efforts	Reddy
	Discussion	Li

The "Nuclear Equation of State" workshop attendees

Name	Affiliation
Ed Brown	Department of Physics and Astronomy, Michigan State University
Zbigniew Chajecki	Western Michigan University
Katerina Chatziioannou	Center for Computational Astrophysics, Flatiron Institute
Pawel Danielewicz	FRIB, Michigan State University
Umesh Garg	University of Notre Dame
Jeremy Holt	Texas A&M University
Chuck Horowitz	Indiana University
Che-Ming Ko	Texas A&M University
Bao-An Li	Texas A&M University - Commerce
Bill Lynch	FRIB, Michigan State University
Brian David Metzger	Columbia University
J. B. Natowitz	Texas A&M University
Jorge Piekarewicz	Florida State University
David Radice	Princeton University
Madappa Prakash	Ohio University
Sanjay Reddy	University of Washington and INT
Luke Roberts	FRIB, Michigan State University
Ingo Tews	Los Alamos National Laboratory
Betty Tsang	FRIB, Michigan State University
Sherry J. Yennello	Cyclotron Institute, Texas A&M University